Form drag of subaqueous dune configurations

Manfred Jellesma

BSc., Civil Engineering (University of Twente, Enschede)

University of Twente & HKV lijn in water

November 25, 2013

Under supervision of the master thesis committee:

Prof. dr. S.J.M.H. Hulscher
University of Twente, Department of Water Engineering and Management

Dr. J.J. Warmink
University of Twente, Department of Water Engineering and Management

Dr. ir. A.J. Paarlberg
HKV Consultants, Advisor rivers and coasts

Dr. A. Lefebvre
MARUM, Center for Marine Environmental Sciences

Dr. ir. G.H. Keetels
Delft University of Technology, Department of Maritime and Transport Technology

Preface

This master thesis presents the results of a study to the form drag of subaqueous dune configurations in rivers. The research is carried out in cooperation with the University of Twente and HKV Consultants.

I would like to thank all my committee members for helping me out in the past six months. First of all I have to thank Andries Paarlberg for his guiding and support on a daily basis during the research at HKV Consultants. You always had time for my daily problems and helped me out with some out of the box thoughts. Secondly I have to thank Alice Lefebvre for sharing her knowledge and results on dune modelling in Delft3D. Thanks for your supporting and always encouraging e-mails. From the University of Twente I thank Jord J. Warmink and Suzanne J.M.H. Hulscher for their guidance during the preparations of the master thesis and for giving critical reviews and structure to the research later on. The last committee members I have to thank is Geert H. Keetels. I really appreciated your unconditional help on OpenFOAM, although you joined the committee later.

Other than my committee, I have to thank my unofficial committee member, Fredrik Huthoff as well for his guiding and support at HKV Consultants. Thanks for learning me the basics and some useful features of OpenFOAM. Finally I want to show my gratitude to HKV Consultants for giving me the opportunity to conduct this research and facilitating the working environment.

Abstract

In hydrodynamic modelling of river flows a key model parameter is the hydraulic roughness of the river bed, which is related to grain characteristics of the bed and the geometries and spatial distribution of bed forms. This parameter is commonly used for model calibration, where stationary roughness coefficients are chosen such that an accurate match between modelled and empirical flow data is achieved. However, from existing bathymetric measurements it is known that bed forms take on different shapes during the passage of a discharge wave. These observations of changing bed forms therefore indicate that bed roughness is not a stationary variable (as assumed in many hydrodynamic river models), but rather that bed roughness responds to hydrodynamics. It appears that during the rise of a discharge wave the bed forms tend to grow in height and length, and that bed forms tend to merge and decay during the falling stage of a discharge wave.

The objective of this research is to investigate the form drag of several idealized dune configurations in order to provide a better understanding of roughness variability during flood waves. Therefore the software package OpenFOAM is used to set up a non-hydrostatic numerical 2DV (two dimensional vertical plane) flow model for flow over dunes. The form drag of the several dune configurations is determined from this model, which is then used to describe the roughness variation during flood waves. In total three, on measurements based, dune configurations are investigated: (1) secondary dune, (2) primary dune and (3) primary dune consisting of merged secondary dunes.

The model is validated by theoretical logarithmic straight bed flow and by measurements of single dune shape laboratory experiments. The straight bed case fits the logarithmic velocity profile well and the roughness parameter based on the flow properties of the model is in accordance to the input of the model. For the dune shapes, a calibration and validation case are carried out. The calibration case estimates the grain roughness of the concrete material used in the experiments, while the validation case shows the performance of the model. Both modelled dune cases show high agreement to measured velocity profiles, flow separation zone and total roughness parameters.

Form drag of the investigated dune configurations appears to increase for increasing dune length and height. The form drag increases as well for the same primary dunes but consisting of merged secondary dunes. It appears the form drag of primary dunes consisting of merged secondary dunes is slightly higher than the summation of the form drag of each separate bed form. In perspective to the varying bed forms during passing of a discharge wave, it is concluded the form drag of the river bed increases during the rise of a discharge wave. For the falling stage of a discharge wave it is concluded the form drag may still increase. Secondary dunes merged on primary dunes add a significant amount of form drag, but the effect of decay of primary dunes in this stage is not determined. It depends on actual primary and secondary bed form shape and dimensions if form drag increases or decreases during the falling stage.

Contents

List of Figures

List of Tables

Chapter 1

Introduction

In The Netherlands the flood defence system of rivers is based on the occurring water levels during a certain high discharge event. This high discharge event, the design discharge, is coupled to a very low chance of occurrence following the Dutch regulation. Since no field data are available of such rare events, existing discharge measurements are extrapolated in order to find the discharge given a certain chance. The design water levels follow from numeric models, using this design discharge as boundary condition.

In numeric models the discharge wave, river dimensions and roughness of the bed are the key parameters controlling the water levels. While the discharge wave and river dimensions can be reasonably estimated, much is yet unknown about the bed roughness in rivers. Therefore, the bed roughness parameters are often used to calibrate the models using fixed roughness parameters in time.

However, several researchers (e.g. Julien et al. (2002); Wilbers and Ten Brinke (2003)) indicate that the bed roughness parameters are likely to change with varying discharge. The changing flow conditions during a discharge wave (flow velocities and water depth) influence the sediment transport at the river bed and therefore cause for different bed forms to occur. It is likely that these bed forms cause the river bed roughness to change, which is in contradiction to the fixed roughness parameters used in the numerical models for the prediction of water levels.

This chapter explains the main characteristics of bed forms, river bed roughness and defines the research objective of this research.

1.1 River bed forms

River bed forms develop due to the interaction between flow and a moveable bed. For a flow over an initial plane bed, if sediment transport occurs, the bed may become unstable and bed forms start to develop (Engelund, 1967). Dunes are typical bed forms arising at the river bed. Dunes occur in different dimensions and shapes which all mainly depend on water depth, flow velocity and sediment properties. For this research the shape of the dunes is assumed to be asymmetrical. Typical asymmetrical dunes consist of a gentle stoss side and a relatively steep lee side (figure 1.1). Other important dune properties are the dune length and the crest height.
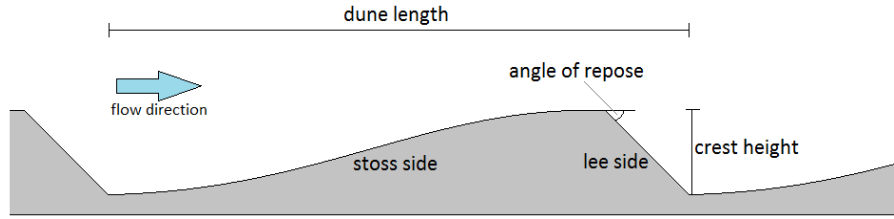
Figure 1.1: Properties of subaqueous dunes

Assuming the sediment properties do not change during a discharge event, the dune dimensions mainly depend on water depth and flow velocity. Under, steady conditions, erosion towards the crest equals deposition just after the crest and dune dimensions are in equilibrium. Dunes then migrate in the direction of the flow (for Froude numbers smaller than 1) (Knighton, 1998). However, in most rivers discharge is constantly changing and therefore no equilibrium situation is reached. In fact, due the slow morphological processes, the bed is in constant movement towards a new equilibrium situation.

Warmink et al. (2012) stated different hypothetical stages of bed forms during a discharge wave, which are believed to show a general pattern of bed forms during discharge waves in rivers (figure 1.2). In these stages a hysteresis in bed forms and discharge is clearly visible (also observed by Julien et al. (2002); Wilbers and Ten Brinke (2003)). During low discharge dunes are small, but they grow larger with increasing discharge. When the peak discharge has passed, dunes continue to grow due to the lagged adaptation of sediment processes to flow properties. At the end of the discharge wave the dunes become lower and smoother (lower angles) but keep increasing in length. In this phase smaller dunes (secondary dunes) start to arise on top of these dunes.

1.2 River bed roughness

The roughness of a river depends on all of the induced resistances to the flow. The flow resistance is for example influenced by vegetation, bed material, bed shape or structures (groynes, bridges). However, in theoretical research the roughness of rivers is assumed to consist of only bed roughness. Bed roughness is the total roughness to the flow induced by the river bottom. The roughness of the banks of a river are often neglected, which is appropriate when dealing with relatively wide rivers. The total river roughness is for this research assumed to consist of only the bed roughness. The two main components of bed roughness consists of grain friction [1] and form drag [2] (e.g. Ogink (1989); Julien et al. (2002)).

1.2.1 Grain roughness

Grain roughness refers to resistance to flow due to the shear stress applied on individual grains on the river bed (Julien et al., 2002). For a turbulent flow subjected only to grain

---

[1]Grain roughness results from resistance to flow due to the shear stress applied on individual grains.
[2]Form drag results from pressure gradients in the flow which induces turbulence and leads to energy dissipation.
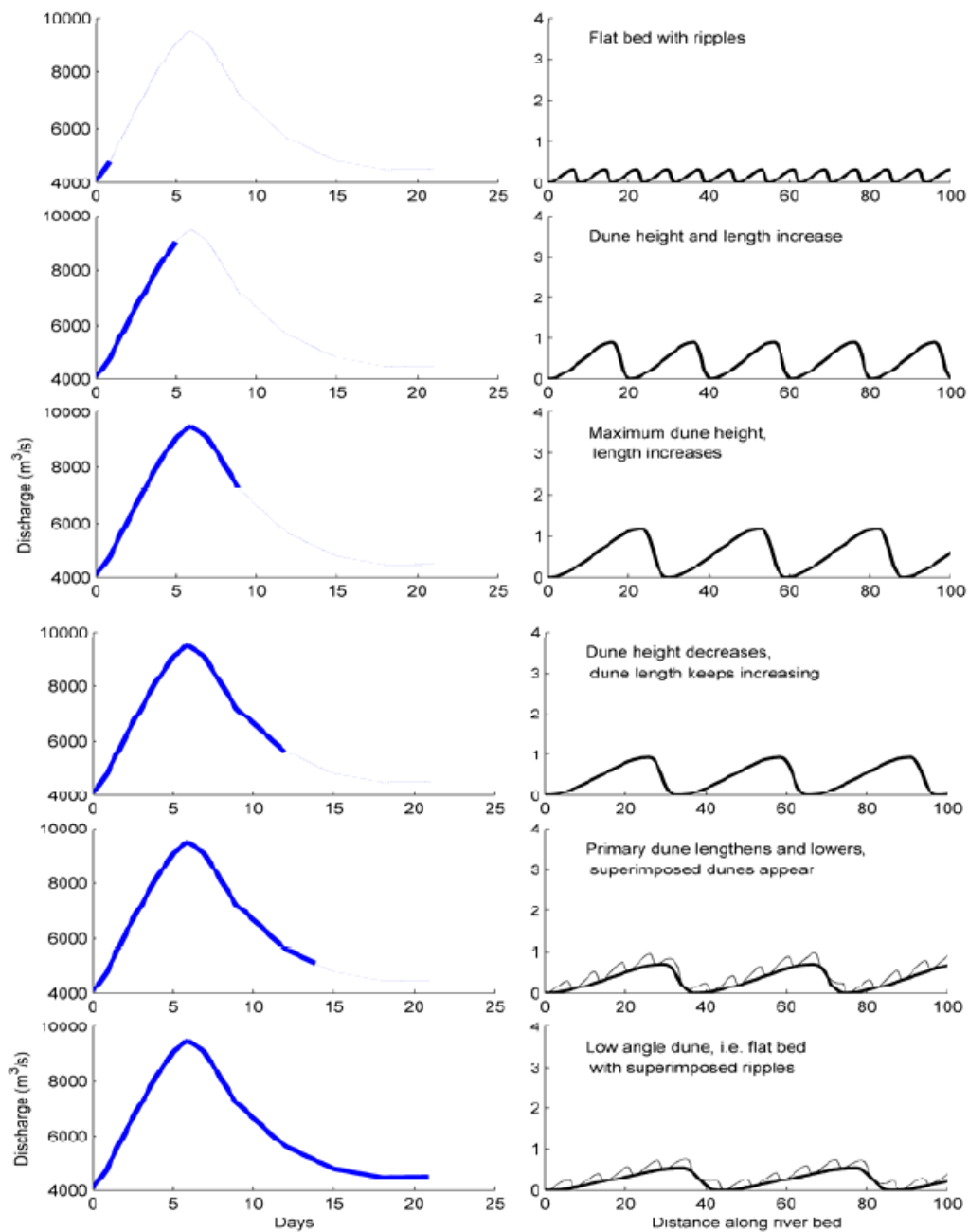
Figure 1.2: Proposed model of bed form evolution under varying discharge in flume and field (Warmink et al., 2012)

roughness the velocities are theoretically approximated by a logarithmic velocity profile (van Rijn, 1993) for which several regions are distinguished (figure 1.3). The viscous sub-layer is a very small laminar layer close to the wall where viscous shear stresses dominate (Booij, 1992) and the velocities at the wall are usually assumed to be zero (Knighton, 1998). In this region the velocity gradient is approximately linear (Booij, 1992). The buffer region is a transition layer from laminar to turbulent flow where both the viscous and turbulent stresses are important (Booij, 1992). In the fully turbulent region turbulent

stresses dominate (Booij, 1992) and velocity varies semi-logarithmically with the water depth (Knighton, 1998). This layer extends over 10 to 20 per cent of the water depth. The upper 80 to 90 per cent consists of the outer layer, where large scale turbulence is present and the velocity profile diverges from a semi-logarithmic form (Knighton, 1998).
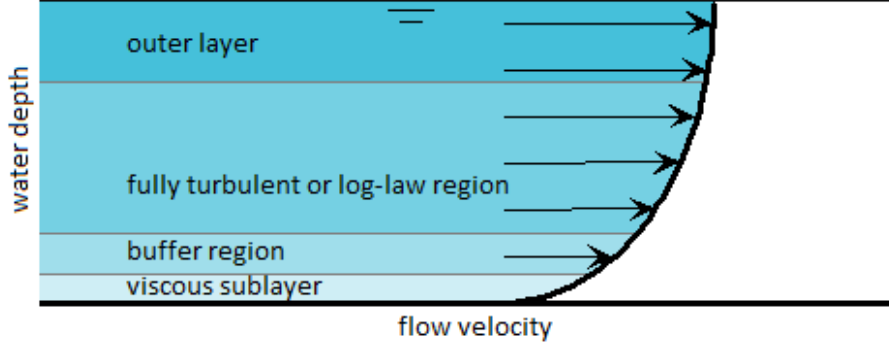
Figure 1.3: Flow regions for a turbulent flow over a straight bed

Grain roughness properties of the bed can be expressed by the Nikuradse roughness length k_s and roughness height z_0. Expression of the Nikuradse roughness length into roughness height depends on the roughness regime. The dimensions of grain particles at the river bed often exceed the height of the viscous sublayer and the flow regime is hydraulically rough. For flows where the grain particles of the bed do not exceed the size of the viscous sublayer the flow is defined as hydraulically smooth. The mathematical definition of the hydraulically rough and smooth regime are given by equation 1.1 and 1.2 (van Rijn, 1993):

$$\frac{k_s u*}{\nu} >> 1 \tag{1.1}$$

$$\frac{k_s u*}{\nu} << 1 \tag{1.2}$$

$k_s = Nikuradse\ roughness\ [m]$
$u* = shear\ velocity\ [m/s]$
$\nu = kinematic\ viscosity\ [m^2/s]$

For this research all flow regimes meet the hydraulically rough condition.

1.2.2   Form drag

The flow over an asymmetric dune separates at the crest, creating a large separation zone in the trough. According to Paarlberg et al. (2007) the main turbulence pattern behind a dune consists of a circular flow, called the flow separation zone, which is most influenced by the dune height and the angle at the flow separation point. The difference in pressure between the stoss and lee sides produces a net force on the dune called form drag (Maddux et al., 2003).

Best (2005) summarized five major regions in flow over river dunes. These region apply to asymmetrical dunes with an angle-of-repose lee side and are generated in a steady, uniform unidirectional flow.

Regions in flow over asymmetrical dunes:

1. A region of flow separation is formed in the lee of the dune

2. A shear layer is generated bounding the separation zone

3. A third region is one of expanding flow in the dune lee side

4. New internal boundary layer grows as flow re-establishes itself

5. Maximum horizontal velocity profile occurs of the dunes crest
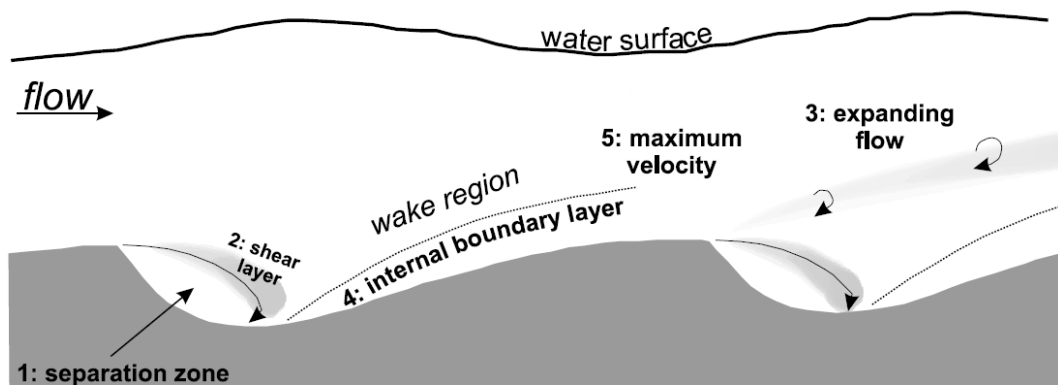
Figure 1.4: Schematic representation of the flow regions in flow over dunes (Best, 2005)

Figure 1.4 visualises flow separation at the crest and circular flow in the trough of the dune. Behind the flow separation zone a wake region arises, covering high turbulences in the flow. The flow separation zone is therefore of high importance for the amount of form drag. On the stoss side the flow recovers from turbulences and reaches maximum velocities towards the crest.

1.2.3 Turbulent kinetic energy

The grain roughness and the form drag of the river bed both induce turbulences which results in resistance to the flow. The Turbulent Kinetic Energy (TKE) is defined by the mean kinetic energy associated with these turbulences in the flow. Cross sectional plots of the TKE are therefore useful for showing the location and intensity of turbulence. In particular for form drag the TKE reveals high turbulent regions in the water column, like the wake region visualised in figure 1.4.

1.3   Research objective

The objective of this research is defined:

To provide a better understanding of the roughness variability during flood waves, by computing the form drag of typical primary and secondary dune configurations in rivers.

Typical occurring dune configurations refer to the 6 stages of the bed form evolution process during a flood (chapter 1). By making use of 2DV (two dimensional vertical plane) numerical modelling, the flow over typical bedforms is simulated and the output flow properties are used to derive the form drag.

The numerical modelling is conducted using the CFD (Computational Fluid Dynamics) software package OpenFOAM. OpenFOAM is open source, therefore free to use, and provides the ability of constructing and computing 'flexible' meshes. This means the mesh can be locally refined without increasing the mesh resolution of the whole domain.

1.3.1   Research questions

In order to give guidance to the research objective, the following research questions are defined:

1. Which model settings are used for creating a free surface model in OpenFOAM?

2. How do the model results compare to a validation reference case?

3. What is the form drag of the investigated dune configurations?

4. What are the variations in form drag during floods, following the proposed model of bed form evolution (figure 1.2)?

1.3.2   Structure of the report

A short overview of the structure of the report is given below:

- Chapter 1: Introduction
  General introduction to river bed forms, river bed roughness and definition of the research objective.

- Chapter 2: Methods
  Describes the free surface OpenFOAM model and the general model settings. Besides the general flow conditions and the method of form drag and grain roughness determination is explained.

- Chapter 3: Model calibration and validation
  The fundamentals of the free surface OpenFOAM model are validated by the logarithmic velocity profile over a straight bed. Next, the model is calibrated and validated by measurements of laboratory experiments of flow over dunes.

- Chapter 4: Model experiments
  Three experimental dune configurations are defined and the resulting modelled flow over these bed forms is discussed.

- Chapter 5: Discussion
  The results of experimental dune configurations are discussed in perspective to variations in form drag of the proposed dune evolution process. Besides the influence of the most important assumptions of the model and the bed forms is explained. The last part of this chapter proposes several recommendations for improvement of the model set up.

- Chapter 6: Conclusions and recommendations
  The general conclusions of the research are summarized by answering the research questions. Besides several recommendations for future research are proposed.

Chapter 2

Methods

This chapter explains the model settings, flow conditions and method used for deriving the form drag from flow properties.

2.1 Set up of the model

The main parts of the model are explained in this section. OpenFOAM is shortly introduced after which the boundary conditions, solver and turbulence model are discussed. The last part explains the grain roughness specification in the free surface model and the construction of the mesh.

2.1.1 OpenFOAM

OpenFOAM is a multi-dimensional open source CFD (Computation Fluid Dynamics) which has a wide range of standard solvers for different flow conditions. However, fundamentally OpenFOAM is a tool for solving partial differential equations rather than a CFD package in the traditional sense. Therefore it can also be used in other areas like stress analysis, electromagnetic and finance (OpenFOAM Foundation, 2013).

For the purpose of this research OpenFOAM is used to set up a 2DV (two dimensional vertical plane) free surface flow by modelling both water and air particles.

2.1.2 Boundary conditions

Boundary conditions need to be chosen properly, since they are of high importance to the model and have a high influence on model output. The boundary conditions for the model are separated into hydraulic and spatial boundary conditions. Hydraulic boundary conditions are boundaries applicable to water and air, while spatial boundary conditions refer to the spatial domain of the model.

Hydraulic boundary conditions

The inlet and outlet of the model consist of 'cyclic' boundary conditions. This means that the flow and its properties that exit the model, enter the model at the inlet. The

advantage gained by using cyclic boundary conditions is that for repetitive bed forms the model domain is kept small. The ceiling of the model, called 'atmosphere', consists of an 'inlet-outlet' boundary condition. Therefore air is allowed to flow in or out at this boundary. The bottom boundary condition is set to the type 'wall'. By specifying the bottom boundary as 'wall', wall functions are applicable to this boundary and roughness can be specified. The utility of wall functions and the addition of a certain roughness to the boundary is explained in section 2.1.6. More technical details of the boundary conditions used in the model are found in appendix A. A schematic representation of the model is shown in figure 2.1 and 2.2.
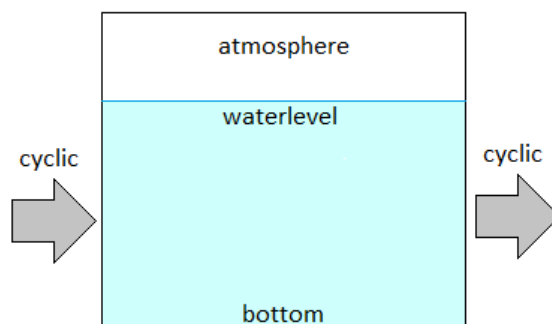
Figure 2.1: Schematic model setup (flat bed case)
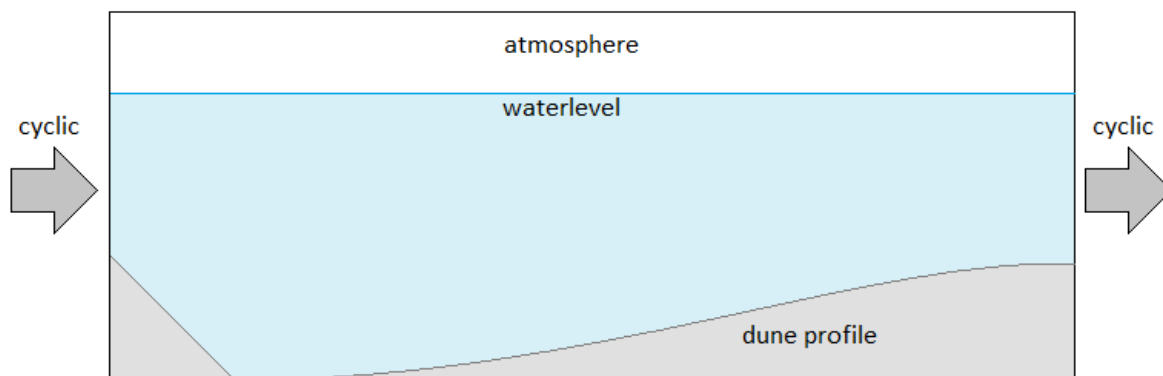
Figure 2.2: Schematic model setup (dune case)

Spatial boundary conditions

Due the use of cyclic boundary conditions, the spatial domain of the model can be limited to include one bed form (figure 2.2 illustrates this). Therefore the domain length depends on the length of the bed form. The model height depends on the water level and the thickness of the atmospheric layer above the water surface. In all cases the thickness of the atmospheric layer is modelled by 10 equally sized cells, which have the same dimensions as cells just below the water surface.

2.1.3 Adapted interFoam solver

OpenFOAM contains many solvers for different purposes. The interFoam solver is used in this research, since the interFoam solver is able to model the behaviour of two incompressible fluids. In the context of hydraulic flow modelling, these two fluids consist of water and air. The interest for this research lies in the modelling of water particles. However by modelling the air particles as well, a free water surface is created.

The standard interFoam solver is not able to model a free surface flow using cyclic boundary conditions. To make the interFoam solver work properly with cyclic boundary conditions, the flow needs to be driven by a horizontal force.

The interFoam solver solves the Reynolds-Averaged Navier-Stokes (RANS) equations, which consist of the continuity equation (equation 2.1) and momentum equation (equation 2.2) (Liu et al., 2008). In order to generate a horizontal forcing on the flow an extra term ($\rho\, Bodyforce$) on the right hand side is added to the momentum equation. The 'Bodyforce' parameter defines the size and direction of a force. Therefore this force consists of an x-, y- and z-component. For the purpose of 2DV free surface flow only a flow in x-direction is needed. The size of the force is defined by the gravitational force times the bed slope of the channel (equation 2.4).

$$\nabla \cdot u = 0 \tag{2.1}$$

$$\frac{\partial \rho u}{\partial t} + \nabla \cdot (\rho u\, u) - \nabla \cdot ((\mu + \mu_t)S) = -\nabla p + \rho g + \sigma K \frac{\nabla \alpha}{\mid \nabla \alpha \mid} \tag{2.2}$$

$u = velocity\ vector\ field$
$\nabla = divergence\ in\ the\ x-,\ y-\ and\ z-direction$
$p = pressure\ field$
$\mu = viscosity$
$\mu_t = turbulent\ eddy\ viscosity$
$S = strain\ rate\ tensor$
$\alpha = volume\ fraction\ (0:\ air,\ 1:\ water)$
$\sigma = surface\ tension$
$K = surface\ curvature$

$$\frac{\partial \rho u}{\partial t} + \nabla \cdot (\rho u\, u) - \nabla \cdot ((\mu + \mu_t)S) = -\nabla p + \rho g + \sigma K \frac{\nabla \alpha}{\mid \nabla \alpha \mid} + \rho\, Bodyforce \tag{2.3}$$

$$Bodyforce = (\quad \underbrace{ig}_{x-component} \quad \underbrace{0}_{y-component} \quad \underbrace{0}_{z-component} \quad) \tag{2.4}$$

The entire code of the adapted interFoam solver can be found in appendix B.

2.1.4   Turbulence model

OpenFOAM supports a wide range of turbulence models. In this research the conventional k-epsilon turbulence model is used to simulate turbulence. In this model k defines turbulent kinetic energy, while ϵ expresses the turbulent energy dissipation rate. The k-epsilon turbulence model is a high Reynolds number turbulence model, which means the model can not solve the flow entirely to the wall (where the Reynolds number is low). Therefore wall functions are applied to the first cells at the wall boundaries, which give the ability of applying a certain roughness to these walls. The values of the turbulence parameters of the k-epsilon model are not changed and have default values programmed in OpenFOAM:

$C_\mu = 0.09$
$C_1 = 1.44$
$C_2 = 1.92$
$\sigma_\epsilon = 1.3$

In an earlier stage of this research also the k-ω SST turbulence model was applied. The SST k-ω model is a combination of the k-epsilon model (for high Reynolds number modelling) and the k-ω model (for low Reynolds number modelling). This makes the SST k-ω turbulence model suitable for modelling both laminar and turbulent regions of the flow (section 1.2.1). For this research however, the time to solve the flow entirely to the wall would take to much time in perspective to the improvement in accuracy. Therefore wall functions were applied, but during the model validation the k-epsilon model proved to model the flow separation zone more accurately. This is remarkable since both the k-epsilon and the k-ω SST model should perform alike in high turbulent zones. However, according to Moradnia (2010), not meeting the y+ requirements (section 2.1.6) in the model results in impaired results for the k-omega SST model in contrast to the k-epsilon model. Some areas of the dune profile (close to the dune trough where flow velocities are low) do not satisfy the y+ requirements during the dune validation, which may explain the better performance of the k-epsilon model.

2.1.5   Grain roughness implementation

Due the use of the k-epsilon turbulence model the grain roughness of the bottom in the model is applied by wall functions. The grain roughness is defined by two parameters, the roughness constant c_s and the roughness height k_s. The roughness height and the roughness constant together specify the z_0 at the bottom according equation 2.5 (e.g. Pattanapol et al. (2007); Martinez (2011)). The equation shows that it is possible to specify the same roughness z_0 by different parameter values for c_s and k_s.

It may sometimes be useful to change the roughness constant c_s in order to meet the ratio requirement between the first cell height and the roughness described in section 2.1.6. The value of c_s may vary from 0.5 to 1.0 according to OpenFOAM Foundation (2012), however (Pattanapol et al., 2007) states that the same roughness implementation (2.5) is used for Ansys Fluent but the roughness constant is fixed to a value of 0.327. Sensitivity analyses for the flat bed validation (section 3.1.2) show that the use of a roughness constant value of 0.327, 0.5 or 1.0 makes no difference if the roughness height (z_0) in those cases is maintained. Except for these sensitivity analyses, all cases modelled in this research are conducted using a roughness constant value of 1.0.

$$k_s = \frac{E}{c_s} * z_0 \qquad (2.5)$$

$k_s = roughness\ height\ [m]$
$E = empirical\ parameter\ [-] = 9.793$
$c_s = roughess\ constant\ [-]$
$z_0 = roughness\ length\ [m]$

2.1.6   Construction of the mesh

Creating an appropriate mesh is of high importance for both model output and calculation time. Therefore a set of guidelines and restrictions are defined for creating a mesh. The guidelines are based on the research of Lefebvre et al. (2013) and give guidance in the amount of grid cells needed in the flow separation zone and the water column. However, it should be noticed the research of Lefebvre et al. (2013) is carried out in Delft3D (modelling one phase: water), while OpenFOAM (modelling two phases: water and air) is used for this research. Therefore applying the same mesh settings may not necessarily lead to good results, but during the validation process it is found they fit for OpenFOAM as well. The restrictions are related to the dimensions of the first cells adjacent to the bottom and are needed in order to correctly model the grain roughness.

Guidelines

A set of guidelines are stated and used for building meshes for the dune cases. By using these guidelines, time consuming sensitivity analyses for finding the optimum mesh settings are avoided. The risk taken by this approach is that the optimum mesh settings for OpenFOAM may require more or even less grid cells. However, the calibration and validation cases (chapter 3) show that using the guidelines give appropriate model results in comparison to measurements and the model has reasonable runtimes.

- Horizontal spacing
  Each dune profile is split into at least 100 profiles (equal distance). This is applied for both primary and secondary dunes.

- Water column
  The area between the water surface and the crest of the dune should consists of 20 layers.

- Flow separation zone
  The vertical distance between de through and the crest of the dune are divided into 30 layers, while another 5 layers are added just above the crest.

Restrictions for cells adjacent to the bottom

To correctly model grain roughness in the model two conditions have to be satisfied. In general these conditions apply to the height of the cells adjacent to a wall. For the free surface model the bottom acts like a wall and the conditions apply to the first cells adjacent to the bottom.

y^+ restriction

The $y+$ value is a dimensionless height parameter which indicates in which region of the flow (section 1.2.1) cells adjacent to the wall are located. In section 2.1.4 it is explained that the k-epsilon turbulence is only able of solving the turbulent region of the flow. Therefore it needs to be avoided that the first cells adjacent to the wall are located in the small viscous sublayer or buffer region.

The mathematical definition of the y^+ value is given in equation 2.6 (e.g. Martinez (2011); Salim and Cheah (2009)):

$$y^+ = \frac{y_p u^*}{\nu} \tag{2.6}$$

$y_p = distance\ from\ the\ cell\ centre\ to\ the\ wall\ [m]$
$u^* = shear\ velocity\ [m/s]$
$\nu = kinematic\ viscosity\ [m^2/s]$

The flow regions are separated by the following y^+ values (e.g. Martinez (2011); Salim and Cheah (2009)):

$y^+ < 5$ Viscous sublayer
$5 < y^+ < 30$ Buffer layer
$30 < y^+$ Turbulent boundary layer

In order to place the cells adjacent to the wall in the turbulent region, minimum y^+ values of 30 have to be reached. Since modelling of the viscous sublayer and buffer layer is avoided, 'wall functions' are required to model the influence of the grain roughness to the flow. Based on the defined grain roughness (according to equation 2.5) wall functions model the flow in cells adjacent to the wall.

k_s **restriction**

The grain roughness for a wall is defined by the roughness height (k_s) and roughness coefficient (c_s) (2.5). The specified roughness height represents the height of protruding particles into the flow. Therefore it is physically logical to place the height of the centre of cells adjacent to walls above the specified roughness height. However, from a modelling perspective the height of a cell centre may be preferred to be smaller. For example, the height of the cells adjacent to the wall may be decreased in order to match the dimensions of other cells nearby.

Martinez (2011) conducted a sensitivity analyses to the distortion of model results in comparison to the fraction of the first cell heights to the roughness height. He concluded that the height of the cell centre of the first cell adjacent to the wall should be at a minimum distance of $0.2k_s$ for undistorted model results. Equation 2.7 shows the mathematical definition of this requirement.

$$y_p = 0.2k_s \tag{2.7}$$

$k_s = roughness parameter [m]$
$y_p = distance from the cell centre to the wall [m]$

2.2   Flow conditions

The flow conditions used in this research are based on common river flow conditions. The research is however carried out using laboratory scale dimensions. Therefore the roughness is small and the slope large relative to real river flow properties. In all cases the flow is subcritical (Froude number < 1), fully turbulent (Reynolds number $\gg 2000$), consists of a free surface and meets the hydrodynamically rough condition (equation 1.1).

Due the cyclic boundary conditions the total volume of water in the domain of the free surface model remains constant. Therefore the average water depth in the domain does not change. Unlike real river conditions the free surface model is not tilted and is horizontally orientated. However, the effect of the slope on the flow is in the free surface model replaced by the horizontal component of the gravity (which is controlled by a predefined slope) to the flow. Therefore the flow is driven by this horizontal force and finds a discharge/velocity equilibrium with the total roughness at the bottom.

2.3   Roughness determination

Flow resistance of the bed is commonly expressed by a Nikuradse or Chézy value. The expressions of these parameters are used to derive an expression for form drag.

The model output of a water flow over specific non moving bed forms gives useful information to derive form drag. Due to the controlled environment in the simulations, the total roughness is entirely contributed to two main components of flow resistance: grain friction and form drag. Therefore the form drag is defined by the difference in total roughness and grain roughness (Van Rijn, 1984):

$$k_{s_{FD}} = k_{s_{TOT}} - k_{s_{GF}} \tag{2.8}$$

$k_{s_{FD}} = form\ drag\ [m]$
$k_{s_{TOT}} = total\ roughness\ [m]$
$k_{s_{GF}} = grain\ roughness\ [m]$

2.3.1   Total roughness

Total roughness of the simulations is determined using the Nikuradse roughness parameter. Therefore the Chézy equation is rewritten to include Nikuradse (only valid for hydrodynamically rough flow). Equations are acquired from (van Rijn, 1993).

Chézy:

$$C = \frac{U}{h^{1/2}S^{1/2}} \tag{2.9}$$

Relation Chézy and Nikuradse:

$$C = 18log(\frac{12R}{k_s}) \tag{2.10}$$

For wide channels where the roughness of the sides can be neglected ($R = h$):

$$C = 18log(\frac{12h}{k_s}) \tag{2.11}$$

Combining equation 2.9 and 2.11 gives the expression for k_s. This equation is used in chapter 3 and 4 to derive total roughness.

$$k_s = \frac{12h}{10^{[\frac{U}{18\sqrt{hS}}]}} \tag{2.12}$$

$C = Chézy\ roughness\ parameter\ [-]$
$U = flow\ velocity\ [m/s]$
$h = water\ depth\ [m]$
$S = water\ slope\ [-]$
$R = hydraulic\ radius\ [m]$
$k_s = Nikuradse\ roughness\ parameter\ [m]$

2.3.2   Grain roughness

Grain roughness is specified at the bottom boundary condition of the model. However, the roughness specified at the boundary will not be used in equation 2.8 in determining the form drag. The grain roughness is derived from the flow velocities of a flat bed case. In this way an error between the specified grain roughness at the boundary and the actual roughness induced in the model is excluded.

Chapter 3

Model calibration and validation

In order to validate the free surface OpenFOAM model two validation cases are modelled. The first validation consists of a flow over a straight bed in order to check the fundamentals of the free surface model. This case is called the flat bed case and experiences only grain roughness. Therefore the flow properties can easily be compared to known theoretical flow physics. After the fundamentals of the free surface model are proven to work, a second validation is carried out comparing the free surface model outcome to measurements of flow over dunes.

3.1 Flat bed validation

The flat bed validation compares modelled velocities to theoretical velocities for flow over a straight bed (figure 2.1). Due the straight bed, total roughness consists of only grain roughness. The grain roughness is specified in the input parameters of the model, along with water depth and bed slope. The runtime of the free surface model is set long enough for the solution to converge and reach a equilibrium state. Convergence of the solution of the free surface model is ensured by monitoring the Courant number and residuals (appendix C). From this equilibrium state, the output flow velocities are used to calculate the grain roughness in the model (equation 2.12). The models works correctly if the derived grain roughness is similar to the grain roughness as specified input parameter. Therefore the difference between the input grain roughness and derived grain roughness is one of the indicators of the performance of the model.

An other indicator of the performance of the model, is to what extent the modelled velocity profile fits the logarithmic velocity profile. The logarithmic velocity profile is defined by equation 3.1 and is controlled by the water depth, water slope and grain roughness (van Rijn, 1993).

$$u = \frac{u*}{\kappa} ln(\frac{h}{z_0}) \qquad\qquad (3.1)$$

$u = velocity\ [m/s]$
$u^* = shear\ velocity\ [m/s]$
$h = water\ depth\ [m]$
$\kappa = Von\ Kármán\ constant\ [-]\ =\ 0.4$
$z_0 = roughness\ height\ [m] = 30k_s$

The flat bed validation is conducted using lab scale dimensions, since the dune validation is carried out on lab scale as well. The following flow parameters are used for the flat bed validation:

$Flat\ bed\ validation\ flow\ parameters$:
$Waterslope = 5 * 10^{-4}\ [-]$
$Water\ depth = 0.5\ [m]$
$k_s = 0.01\ [m]$
$z_0 = \frac{c_s}{E} * k_s$

3.1.1   Model results

The mesh created for flat bed validation consists of 32 cells in the water column, which gradually refine towards the bottom. This is a lot more than required (according to the guidelines in section 2.1.6). However, the air is modelled as well using the same cell size as the water surface. Therefore cells towards the water surface may not get too coarse. The area above the water, the atmospheric region, is modelled by 10 equally sized cells. The mesh and the dimensions of the flat bed model are shown in figure 3.1 and is labelled by 'Flat bed 1a'.

The logarithmic (equation 3.1) and modelled velocity profile are shown in figure 3.2. Close to the bottom, the modelled velocity profiles fits the logarithmic profile very well. However, moving upwards in the water column the modelled profile clearly deviates from the logarithmic profile. In that section the modelled profile ends up vertical, while the logarithmic profile still follows its logarithmic definition (equation 3.1). This is no error in the model, since measurements have shown the velocity profile in a water column consists of both a logarithmic and a parabolic part (Kundu and Ghoshal, 2012). The lower part of the velocity profile acts logarithmic while towards the surface acts increasingly parabolic.

In table 3.1 the average velocity of both profiles are shown. The average velocity of the logarithmic and modelled velocity profile are both numerically determined. From these average velocities the roughness parameters Chézy, Nikuradse and the roughness height z_0 are extracted.

Table 3.1 shows that the average velocity of the logarithmic and modelled profile are slightly different. The derived roughness parameters based on the flow velocities therefore show slight differences. The model performs well with an error of 0.7%. Further, the logarithmic velocity profile does not exactly match the recalculated roughness height. This may be the cause of the chosen κ parameter or small deviations for the assumptions made for equation 2.12.
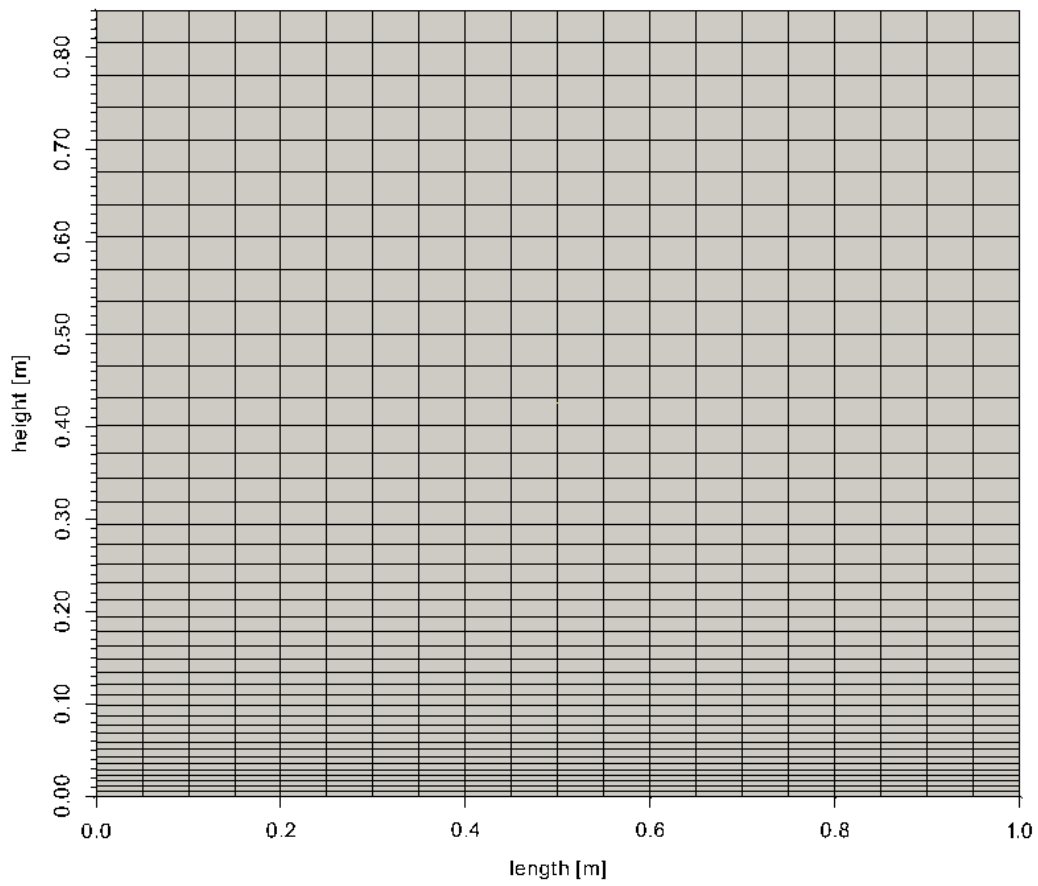
Figure 3.1: Mesh and dimensions of the flat bed validation (Flat bed 1a)
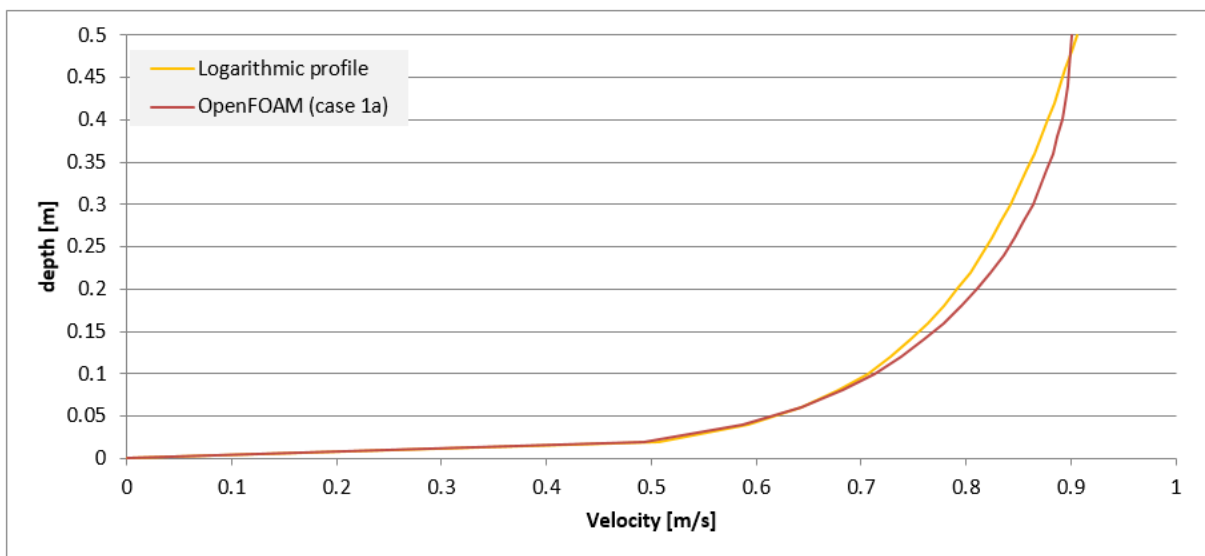
Figure 3.2: Theoretical versus modelled velocity profile (flat bed case 1a)

Table 3.1: Specified roughness (input) compared to the roughness based on the average velocity of the logarithmic and modelled velocity profile (flat bed case 1a)

	input model	logarithmic profile	modelled profile
$\bar{U}$	not specified	0.785	0.792
C	not specified	49.67	50.06
$k_{s\ grain}$	0.01	0.01044	0.00993
$z_{0\ grain}$	0.000333	0.000348	0.000331
difference	-	4.4%	-0.7%

3.1.2   Sensitivity analysis

In numerical modelling the model output is mesh depended. Therefore the magnitude of this dependence should be very small compared to the magnitude of the solution. In order to check the magnitude of mesh dependence of the flat bed validation (flat bed 1a) several mesh adjustments are made (flat bed 2 and 3). However, in some cases (flat bed 1b and 1c) not the mesh dependence, but the influence of the roughness constant (c_s) is determined. In this way equation 2.5 is verified to be valid for OpenFOAM. Besides, two cases (flat bed 4a and 4b) are set up to check some refinement capabilities which are used for the experimental dune configurations in chapter 4. In order to give a full overview of all cases, 'flat bed 1a' is also added to the list below. Besides, in appendix D the mesh for all flat bed cases is visualised.

- Flat bed 1a: c_s value 0.327
  This case is used for the flat bed validation (figure 3.1).

- Flat bed 1b: c_s value 0.5
  This is a copy of 'flat bed 1a', however the roughness constant c_s is changed to 0.5.

- Flat bed 1c: c_s value 1.0
  This is a copy of 'flat bed 1a', however the roughness constant c_s is changed to 1.0.

- Flat bed 2: Surface refinement
  For this case the mesh around the surface is refined. Since the model solves both the water and air particles, it is interesting to check weather the resolution of the transition from water to air influences the modelled velocities.

- Flat bed 3: Total refinement
  For this case the model consists of all equally small cells, to check if the resolution of the mesh in the other cases is fine enough.

- Flat bed 4a: Bottom refinement using SnappyHexMesh
  SnappyHexMesh is a tool which comes with OpenFOAM to adjust meshes. In this case, SnappyHexMesh is used for local refinement at the bottom of the model.

- Flat bed 4b: Partly bottom refinement using SnappyHexMesh In perspective to the dune cases, it is expected the mesh is refined at some specific locations (for example the flow separation zone) and not covering the whole length of the model. Therefore this case tests if the model performs well by partly refining the mesh near the bottom.

The sensitivity of the velocity profiles and derived roughness parameters (equation 2.12) is visualised in figure 3.3 and table 3.2. According to the velocity profiles, the sensitivity of the velocities on the different mesh settings is low. All cases are in high agreement at the bottom, and only have minor velocity differences occur towards the surface. However, these minor differences do have their influence on the average velocity based roughness (table 3.2). From this table, it can be concluded changing the roughness constant (and remaining the value of z_0) does not affect the solution. Further, flat bed 2 and 4b perform the worst, however the differences of respectively 2.8% and -4.2% are still very acceptable. The high resolution mesh of flat bed 3 shows not to perform exceptionally better than the other cases. It performs even slightly worse than flat bed 1, which is expected to be the result of the relatively high aspect ratio of the cells. In contrast to all flat bed cases, flat bed 1a still performs very reasonable.
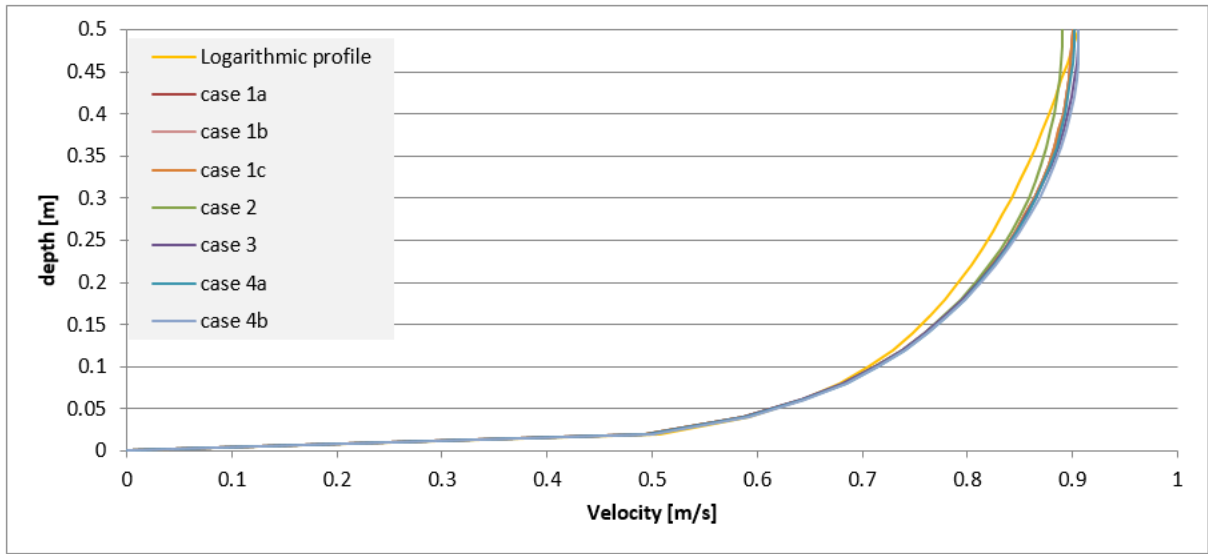
Figure 3.3: Velocity profiles of all flat bed cases

Table 3.2: Sensitivity in grain roughness output parameters

	input model	theoretical profile	Flat bed case						
			1a	1b	1c	2	3	4a	4b
$\bar{U}$	not specified	0.785	0.792	0.792	0.792	0.787	0.793	0.793	0.796
C	not specified	49.67	50.06	50.06	50.06	49.79	50.17	50.19	50.34
$k_{s\,grain}$	0.01	0.0104	0.00993	0.00993	0.00993	0.01028	0.00979	0.00977	0.00958
$z_{0\,grain}$	0.000333	0.000348	0.000331	0.000331	0.000331	0.000343	0.000326	0.000326	0.000319
difference	-	4.4%	-0.7%	-0.7%	-0.7%	2.8%	-2.1%	-2.3%	-4.2%

3.2 Dune calibration and validation

McLean et al. (1999b) conducted a series of laboratory experiments of which one is used for the dune validation. They used concrete to create asymmetric dune shapes. They did not

determine the grain roughness of the material used for these dune shapes. Since the grain roughness is an important input parameter for the free surface model, another experiment of McLean et al. (1999b) is used to calibrate the grain roughness. The roughness obtained from the dune calibration is then used as input for the dune validation.

The second (from now ML2) and sixth (from now ML6) laboratory setup of McLean et al. (1999a) are used for respectively calibration and validation of the free surface model. The ML2 dune case is calibrated on total roughness by adjusting the grain roughness. The total roughness for the flume experiments is derived (making use of equation 2.12) from measured flow velocity, water depth and water slope. The ML6 dune case is validated by velocity profiles, flow separation zone and again the total roughness.

Lefebvre et al. (2013) have modelled all the experiments of McLean et al. (1999b) in Delft3D, therefore the results of OpenFOAM are also compared to the output of Delft3D in appendix E.

- Dune case ML2
  $Dune\ dimensions:\ height\ 0.04\ [m]\quad length\ 0.807\ [m]$
  $Waterslope = 9.5 * 10^{-4}\ [-]$
  $Water\ depth = 0.158\ [m]$
  $Grain\ roughness[1]\ z_0 = 0.00018\ [m]$

- Dune case ML6
  $Dune\ dimensions:\ height\ 0.04\ [m]\quad length\ 0.408\ [m]$
  $Waterslope = 10.2 * 10^{-4}\ [-]$
  $Water\ depth = 0.3\ [m]$
  $Grain\ roughness\ z_0 = 0.00018\ [m]$

3.2.1   ML2 and ML6 mesh

The mesh created for the dune validation is based on the guidelines stated section 2.1.6. However, due the small scale of the experiments, it is hard to meet the y+ requirements for the whole model domain (values of at least 30). The first cell at the bottom would become to large in contrast to the bedform and the other cells. Therefore, the layer added is a compromise of retaining enough accuracy and satisfying the y+ requirement for at least a part of the dune. In this way the top of the stoss side meets the y+ requirements, while in the lee side and the lower part of the stoss side the y+ requirements are not met. This means accuracy is retained at the flow separation zone at the expense of meeting the y+ requirement. This can be justified by the idea that the magnitude of the form drag is greater than the grain roughness. Besides, the flow velocities in the flow separation zone are relatively low and therefore grain roughness plays a less important roll. The mesh created for both the dune validation cases are showed in figure 3.4 and figure 3.5.

---

[1]The grain roughness is found by calibration.
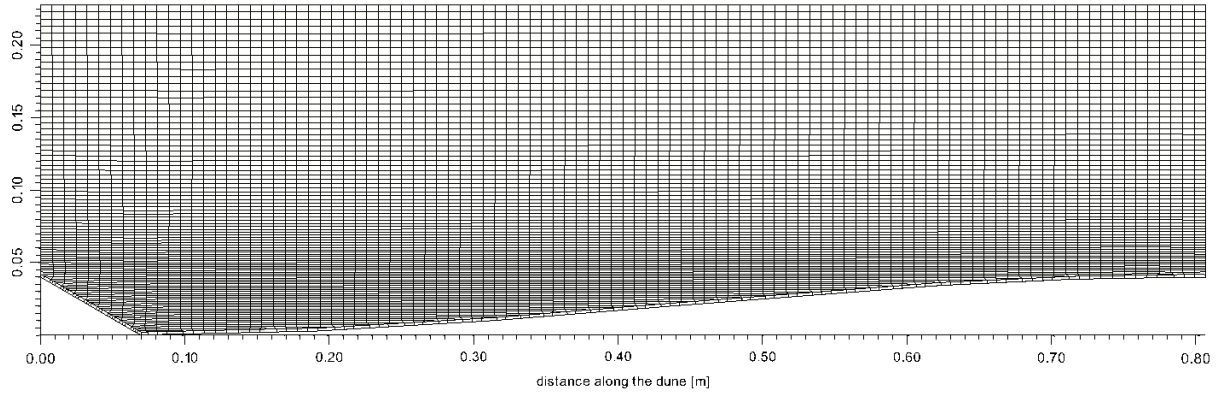
Figure 3.4: Mesh created for ML2 dune validation
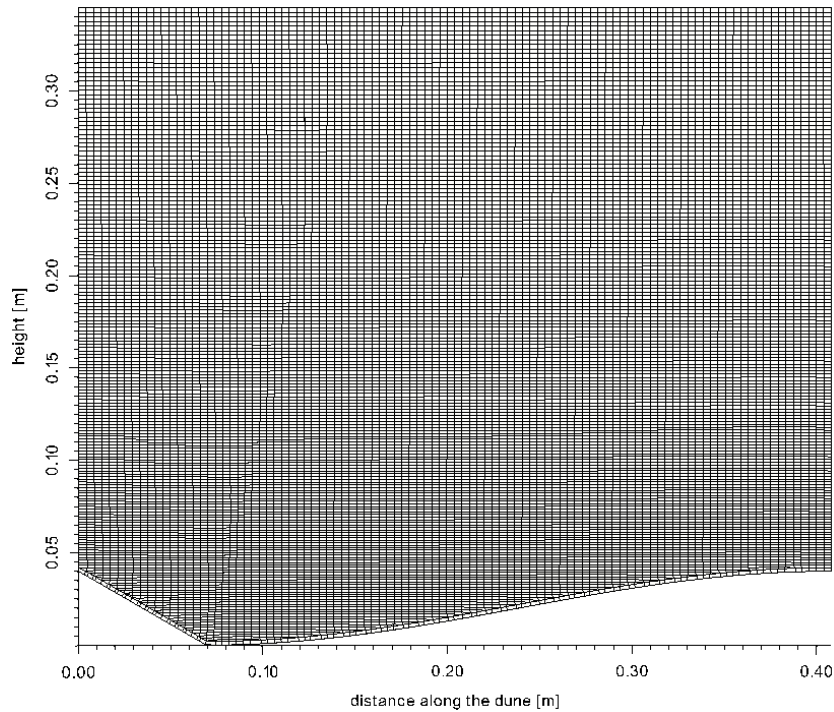
Figure 3.5: Mesh created for ML6 dune validation

3.2.2   Calibration results ML2

The ML2 dune case is used to estimate the grain roughness of the experiments carried out by McLean et al. (1999a). Therefore grain roughness is calibrated to achieve the same modelled total Nikuradse roughness as derived from the ML2 experiment. Lefebvre et al. (2013) used the same case for calibration and found a grain roughness parameter of $z_0 = 0.0002[m]$. This value is used as a starting point, from which the most appropriate value (to use in OpenFOAM) is found to be $z_0 = 0.00018[m]$ (table 3.3).

Calibration of the roughness parameter as shown in table 3.3 is in fact based on the average velocity output of the model only. Therefore the velocity profiles (figure 3.6) and

Table 3.3: ML2 - Calibration of z_0 grain roughness parameter

		measurements	modelled		
input	$z_{0\,grain}$ [m]	-	0.00016	0.00018	0.0002
	slope [-]	0.00095	0.00095	0.00095	0.00095
	depth [m]	0.158	0.158	0.158	0.158
output	$\bar{U}$ [m/s]	0.39	0.395	0.389	0.384
	difference	-	1.33%	-0.16%	-1.49%
	$k_{s\,total}$ [m]	0.0323	0.0306	0.0325	0.0343
	difference	-	-5.65%	0.64%	5.81%
	Chézy [-]	31.83	32.26	31.78	31.36
	difference	-	1.33%	-0.16%	-1.49%

the flow separation zone (figure 3.7) are also compared to the measurements of McLean et al. (1999a). However, these comparisons are only used as a qualitative check.

In general, the modelled velocity profiles are in good agreement with the measured profiles. However, at the stoss side of the dune modelled velocities are underestimated towards the bottom, while they are overestimated in the direction of the surface. On the other hand, the velocity profiles in the flow separation zone show a good fit close to the bottom, but again overestimate the velocity towards the surface. Figure 3.7 verifies that the flow separation zone is accurately modelled. The flow separation zone derived from the measurements is obtained from Paarlberg et al. (2007).

The differences between modelled and measured velocity profiles are likely to be result of the side walls of the flume used in the experiments of McLean et al. (1999a). These side walls are usually made of glass and are very smooth, however they do influence the flow. The model is a 2DV approach of the experiment and therefore these side walls are replaced by empty boundaries. These empty boundaries do not influence the flow. The grain roughness of the side walls and the bottom in the experiment is in the model only represented by the bottom. Therefore it is likely the modelled grain roughness is overestimated to meet the measured average velocity. The velocities towards the bottom are therefore underestimated while the velocities towards the surface are overestimated.

Besides, it is likely there is a slight difference in the ML2 dune shape and the modelled dune shape. It is plausible the experimental ML2 shape had not the exact sinusoidal dune shape, since in figure 3.6 some of the measurements show up inside the bottom profile.
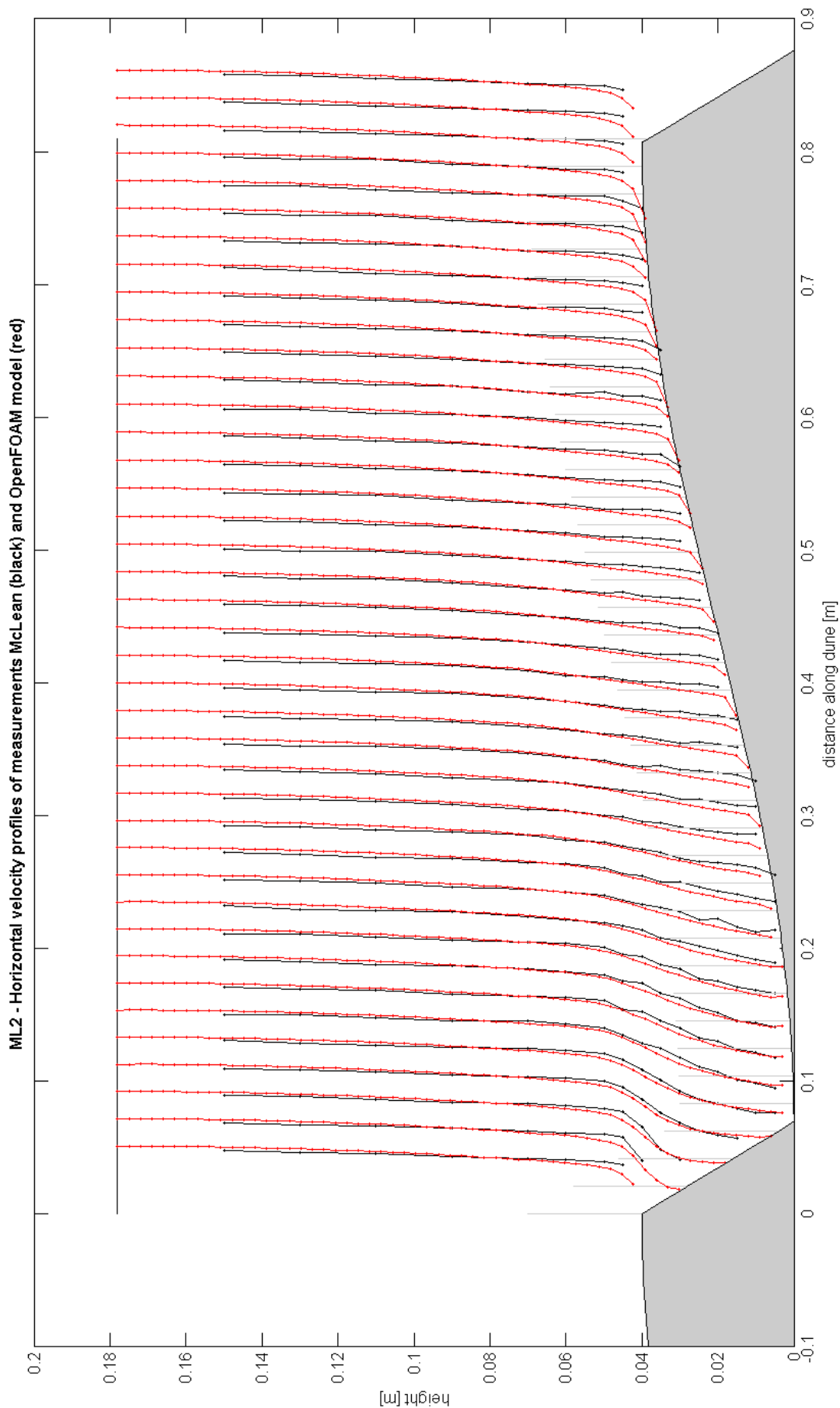
Figure 3.6: ML2 - Velocity profiles of measurements of McLean (black) and modelled by OpenFOAM (red). Velocities are scaled by a factor 10.
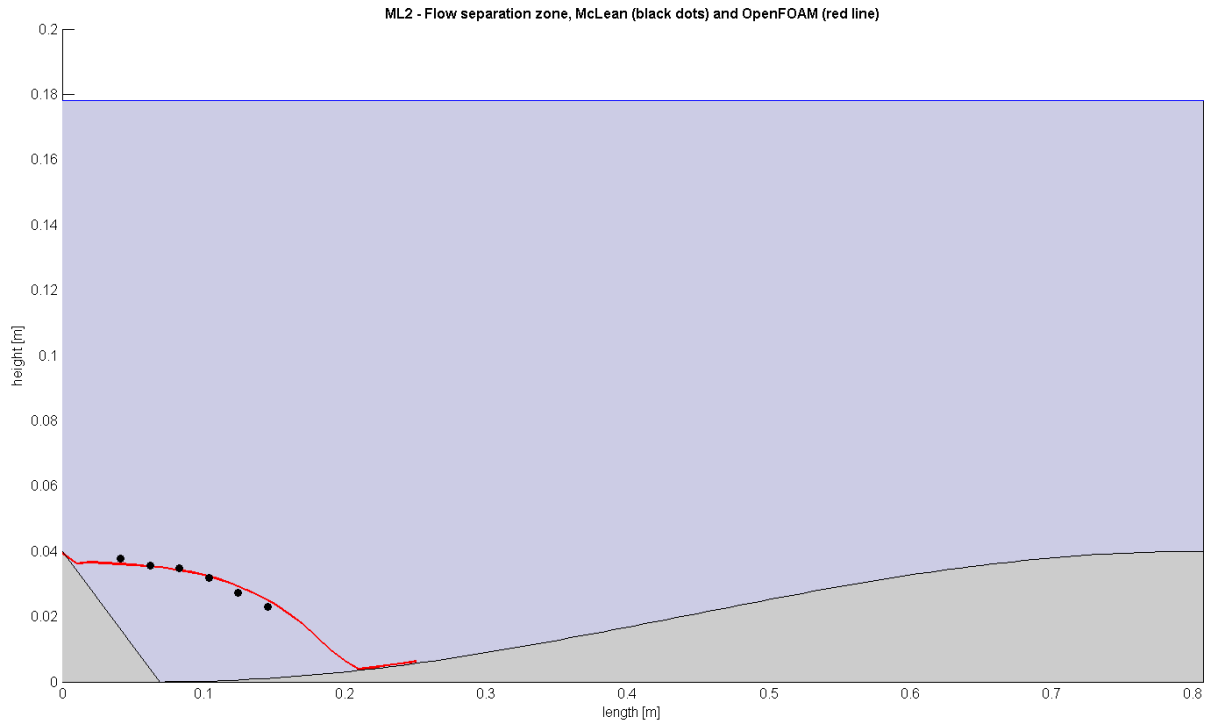
Figure 3.7: ML2 - Flow separation zones of measurements of McLean (black dots) and OpenFOAM (red line)

3.2.3   Validation results ML6

The ML6 case is the actual validation of the model and uses the grain roughness parameter gained from the ML2 calibration case. The flow velocity and total roughness parameters of the modelled ML6 case are shown in table 3.4. The average velocity of the model slightly deviates from the measured flow velocity. The Chézy roughness equation (equation 2.9) takes the average velocity linear into account and therefore the same difference as the average velocity is found in the Chézy roughness parameter. However, the Nikuradse roughness parameter shows a high relative deviation. This does not indicate poor model performance, since the Nikuradse parameter tends to be sensitive to small velocity differences due its logarithmic definition (equation 2.12).

Table 3.4: ML6 - Validation of flow velocities and total roughness

		measurements	modelled	difference
input	$z_{0\,grain}$ [m]	-	0.00018	-
	slope [-]	0.00102	0.00102	-
	depth [m]	0.30	0.30	-
output	$\bar{U}$ [m/s]	0.54	0.561	3.71%
	$k_{s\,total}$ [m]	0.0694	0.0596	-16.44%
	Chézy [-]	30.87	32.06	3.71%

The velocity profiles (figure 3.8) and the flow separation zone (figure 3.9) show still a

good overall agreement with the measurements. Velocity profiles for the modelled and measured ML6 case show similar deviations like the profiles shown for the ML2 case. At the stoss side of the dune close to the bottom the modelled velocities are underestimated, while the modelled velocities towards the water surface exceed the measured velocities. Explanations for these deviations are given in section 3.2.2. Again, the velocity profiles in the flow separation zone fit very well. Figure 3.9 confirms the flow separation zone is decently modelled.

3.2.4   Mesh sensitivity

Section 3.1.2 mentioned that in numerical modelling the output is mesh depended. For the flat bed case several mesh settings were tested to ensure the model output had a low mesh dependency. For the dune validation however, due time limitations, the mesh sensitivity is not tested. Therefore it is explicitly stated the mesh sensitivity of the validation cases remains unknown for this research.

It is important to discuss to which extent this mesh sensitivity might reach. Therefore a view is given on the expectations of the mesh sensitivity for the dune validation cases.

The key property of the guidelines provided by Lefebvre et al. (2013) is to provide enough cells on top of the dune and in the flow separation zone, for the rotational flow to occur. Highly decreasing the amount of cells makes the flow easier to 'attach' the bottom profile in the flow separation zone. Therefore the flow separation decreases or is may be totally absent. Increasing the amount of cells should make the model output more accurate, however the difference in size of the first cell at the bottom compared to the other cells would increase, which may influence the model output as well. For the flow separation zone it is expected that decreasing the mesh resolution would affect the model output the most compared to an increase of resolution.

The water column above the dunes is expected to show only slight dependency to the mesh. The flow in this region is largely horizontal oriented without high turbulence aspects and the increase of the dune over the stoss side is relatively gentle. Therefore this part of the model has some similarities with the flat bed case, which shows a low mesh dependence of the model output.

Analysing the mesh sensitivity of the dune validation cases is in particular useful for the flow separation zone. However, the provided guidelines and the results of both validation cases give confidence in a low, but unknown, mesh dependency.
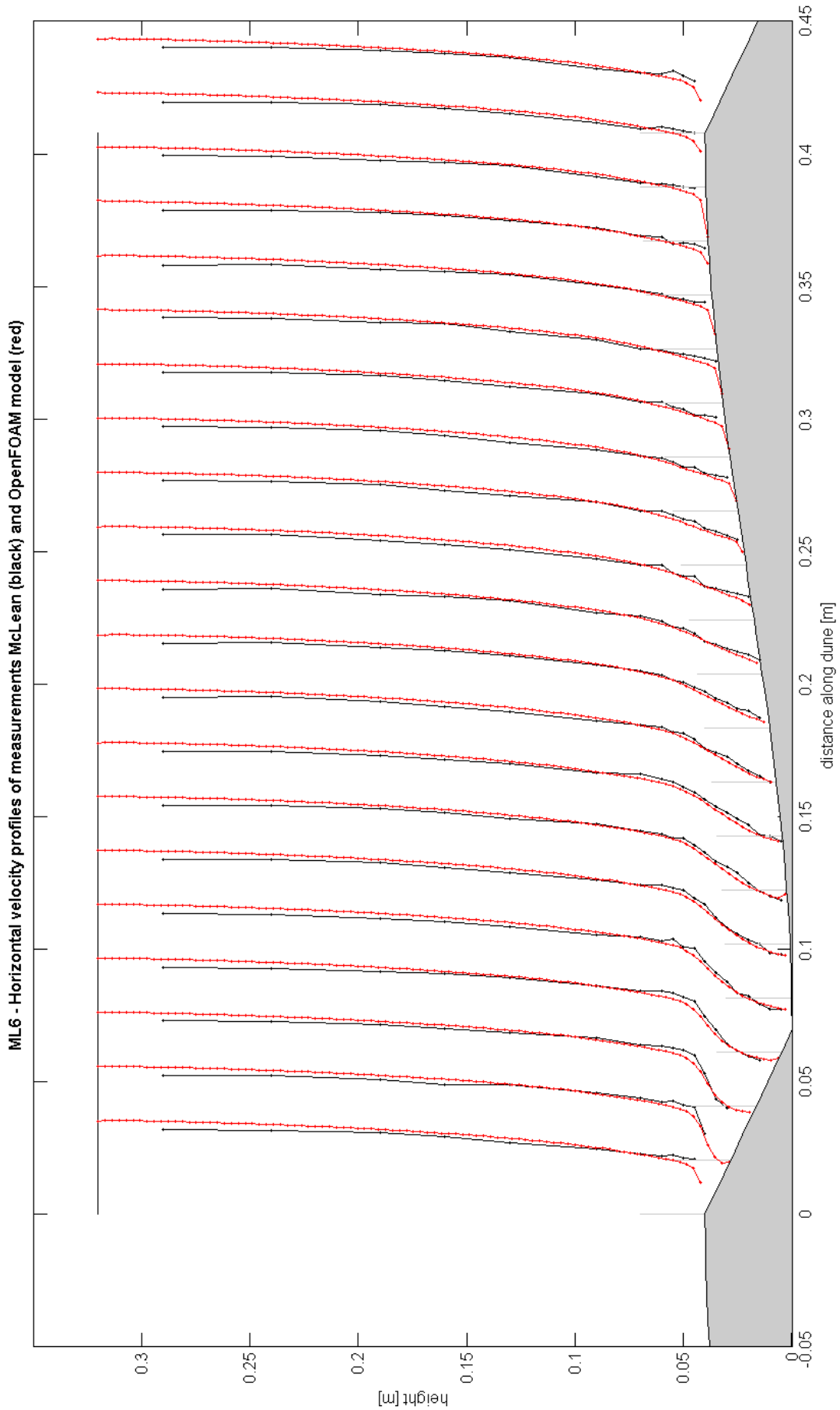
Figure 3.8: ML6 - Velocity profiles of measurements of McLean (black) and modelled by OpenFOAM (red). Velocities are scaled by a factor 20.
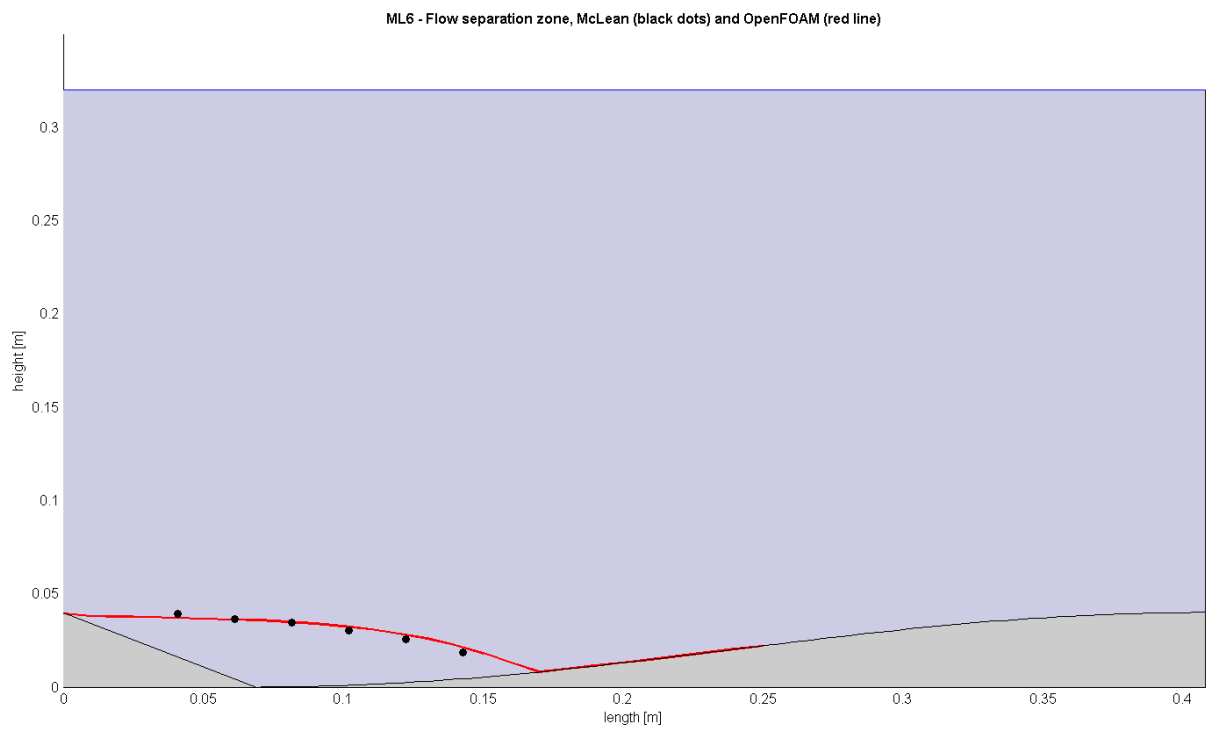
Figure 3.9: ML6 - Flow separation zones of measurements of McLean (black dots) and OpenFOAM (red line)

Chapter 4

Model experiments

The created (chapter 2) and validated (chapter 3) free surface OpenFOAM model is used in this chapter to conduct several experiments. The experiments consist of modelling the flow over different dune configurations which are defined in the first section. In the following sections the model settings, model results and resulting form drag of the experimental dune configurations are discussed.

4.1 Dune configurations

In this section three experimental dune configurations are defined. Dune dimensions and shapes are based on the measurements and shapes discussed in the articles and reports of Julien et al. (2002), Wilbers and Ten Brinke (2003), McLean et al. (1999b), Ogink (1989) and Warmink et al. (2012) (figure 4.1). Therefore, the primary dunes as well as secondary dunes consist of typically sinusoidal stoss sides and straight 30° lee sides. The height and length of dunes is scaled by factor $\frac{1}{10}$ to ensure the dimensions are of the same magnitude as the validation cases (chapter 3).

	Primary dune		Secondary dunes	
Author	Height [m]	Length [m]	Height	Length [m]
Julien et al. (2002)	0.34 - 1.15	8 - 40	0.25 - 0.3	7
Wilbers and Ten Brinke (2003)	0.3 - 1.0	10 - 40		

Author	Dune shape
McLean et al. (1999b)	sinusoidal stoss side and 30° angle of repose
Ogink (1989)	secondary bed forms located more than 6 times the primary dune height away from the point of separation
Warmink et al. (2012)	dune configurations based on proposed bed form evolution process

Figure 4.1: Measured dune dimensions (Julien et al. (2002); Wilbers and Ten Brinke (2003)) and experimental or hypothetical dune shape properties (McLean et al. (1999a); Ogink (1989); Warmink et al. (2012))

The first dune configuration, the 'secondary dune', is a relatively small and short dune. This secondary dune represents bed forms at the first stage of the proposed model of bed form evolution (figure 1.2). The second dune configuration is called the 'primary dune' and consist of a long and high single dune profile. This primary dune is comparable to the maximum dune heights occurring during floods (third stage of proposed bedform evolution model). The third dune configuration consists of a combination of primary and secondary dunes which may be linked to the last two stages of the proposed bedform evolution model. Aside from the dune configurations, a straight bed case is modelled to derive grain roughness of the dune cases.

For all experimental dune configurations and the flat bed case the same flow conditions apply. Therefore grain roughness, average water depth, water slope and bed form volume are remained unchanged for all cases.

Summary of the model experiments:

- Case 0 - Flat bed
  Straight bed. Water level: 0.45 [m] Average water depth: 0.45 [m]

- Dune case 1 - Secondary dune
  Height: 0.03 [m] Length: 0.7 [m] Water level: 0.465 [m] Average water depth: 0.45 [m]

- Dune case 2 - Primary dune
  Height: 0.1 [m] Length: 4 [m] Water level: 0.5 [m] Average water depth: 0.45 [m]

- Dune case 3 - Primary dune containing secondary dunes
  Dune dimensions of primary and secondary dune. Water level: 0.5 [m] Average water depth: 0.45 [m]
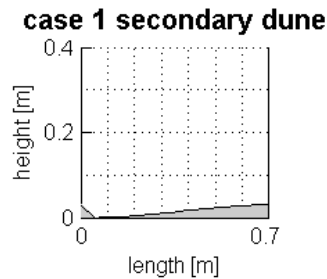
Figure 4.2: Dune case 1: Secondary dune
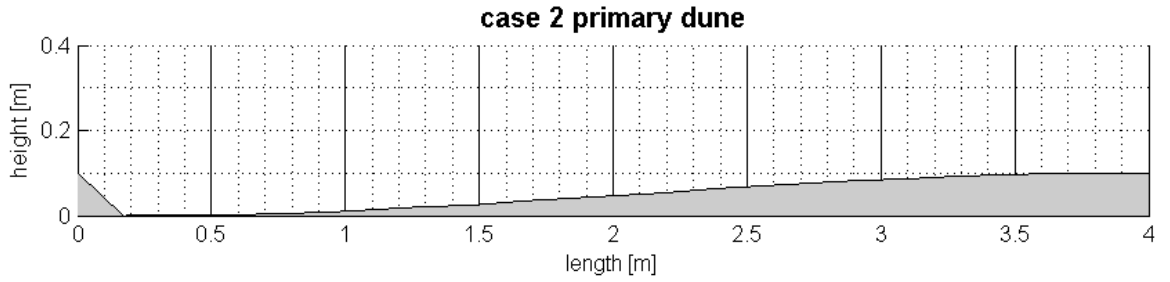
Figure 4.3: Dune case 2: Primary dune
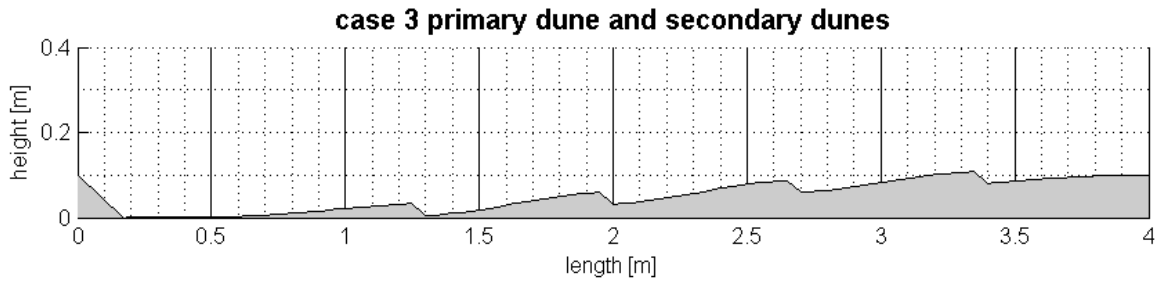
Figure 4.4: Dune case 3: Primary dune containing secondary dunes

4.2 Model settings

This section gives an overview of the model settings for the flat bed case and dune configurations. Grain roughness and water slope settings are adopted from the dune validation case in chapter 3. However, the water depth for the model experiments is increased in perspective to the dune validation case. By raising the water level shear stresses increase which result in higher y^+ values or allows decreased cell heights adjacent to the bottom. This is especially important for the secondary dunes of dune case 3, since the y^+ values get low close to the trough of the primary dune. The constructed meshes for all cases are included in appendix F.

Model settings for the flat bed case and the dune configurations:

- Case 0 - Flat bed
  Water level $= 0.45\ [m]$
  Average water depth $= 0.45\ [m]$
  Waterslope $= 1 * 10^{-3}\ [-]$
  Grain roughness $z_0 = 0.00018\ [m]$

- Dune case 1 - Secondary dune
  Water level $= 0.465\ [m]$
  Average water depth $= 0.45\ [m]$
  Waterslope $= 1 * 10^{-3}\ [-]$
  Grain roughness $z_0 = 0.00018\ [m]$

- Dune case 2 - Primary dune
  $Water\ level = 0.5\ [m]$
  $Average\ water\ depth = 0.45\ [m]$
  $Waterslope = 1*10^{-3}\ [-]$
  $Grain\ roughness\ z_0 = 0.00018\ [m]$

- Dune case 3 - Primary dune containing secondary dunes
  $Water\ level = 0.5\ [m]$
  $Average\ water\ depth = 0.45\ [m]$
  $Waterslope = 1*10^{-3}\ [-]$
  $Grain\ roughness\ z_0 = 0.00018\ [m]$

4.3   Model output

Output of modelled flow for the flat bed case and the experimental dune configurations is covered in this section. For each of the simulations horizontal flow velocities and streamlines are depicted. Streamlines visualise the path of the water particles from which the flow separation zones are easily observed. The air region of the model domain is recognised by the lack of these streamlines.

Turbulent fluctuations induced by the flat bed case and dune cases are visualised by the Turbulent Kinetic Energy (TKE) plots. The intensity of the TKE reveals the high turbulent regions of the flow which contribute to form drag.

4.3.1 Case 0 - Flat bed

Simulation of the flat bed case results in an uniform horizontal velocity field (figure 4.5) and TKE plot 4.6. The streamlines show that flow is horizontally orientated. From the TKE plot is seen TKE increases from the surface towards the bottom. This is the effect of grain roughness acting on the flow. However, in comparison to the dune cases the intensity of the TKE is relatively low.
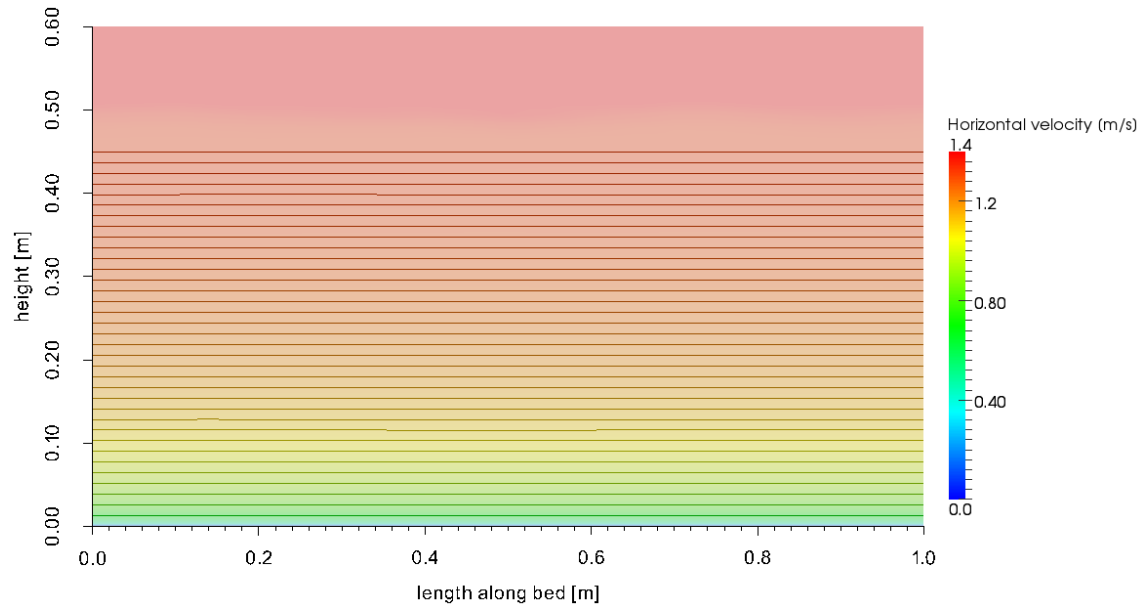
Figure 4.5: Case 0 - Flat bed: Horizontal velocities and streamlines
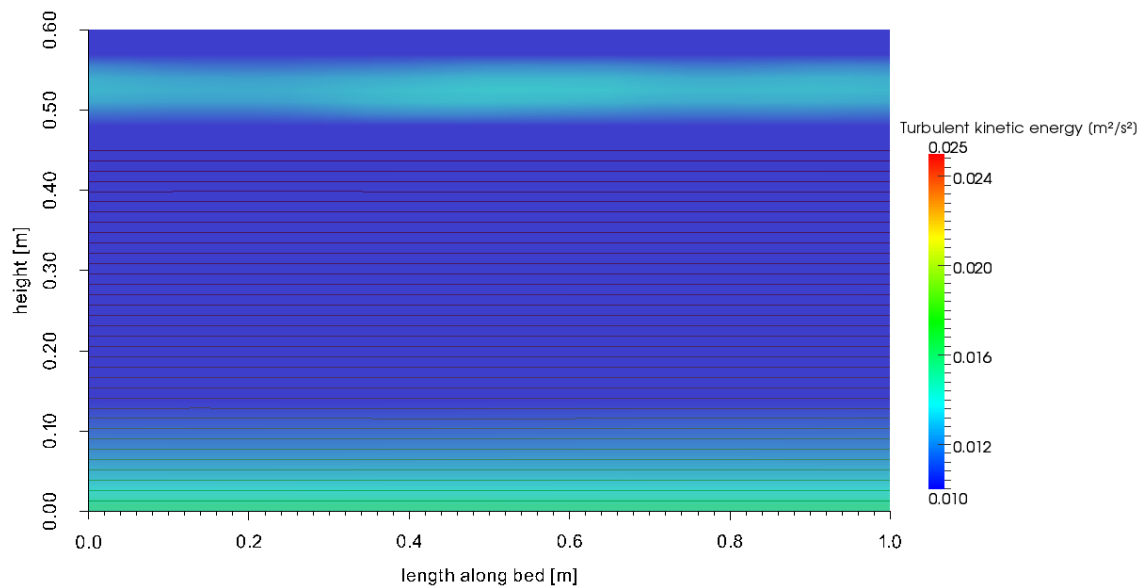
Figure 4.6: Case 0 - Flat bed: Turbulent kinetic energy

4.3.2   Case 1 - Secondary dune

Flow simulated over the secondary dune reveals a disturbance in the flow. Horizontal flow velocities and streamlines (4.7) depict flow separation in the trough of the dune. The TKE plot (figure 4.8) shows that behind the flow separation zone a relative high turbulent region is located in comparison to the flat bed case (case 0). Therefore the flow separation zone highly contributes to the form drag.
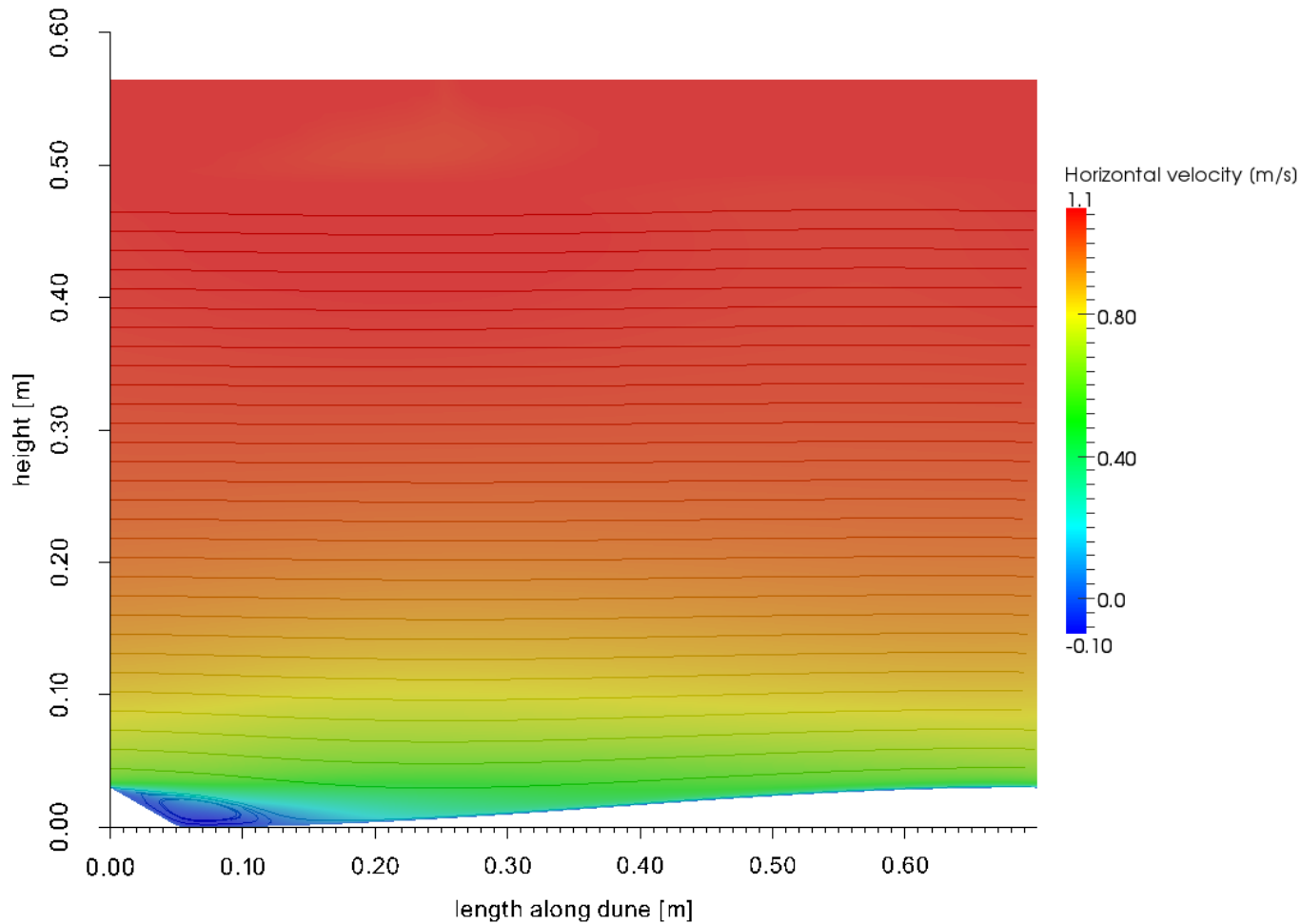
Figure 4.7: Case 1 - Secondary dune: Horizontal velocities and streamlines
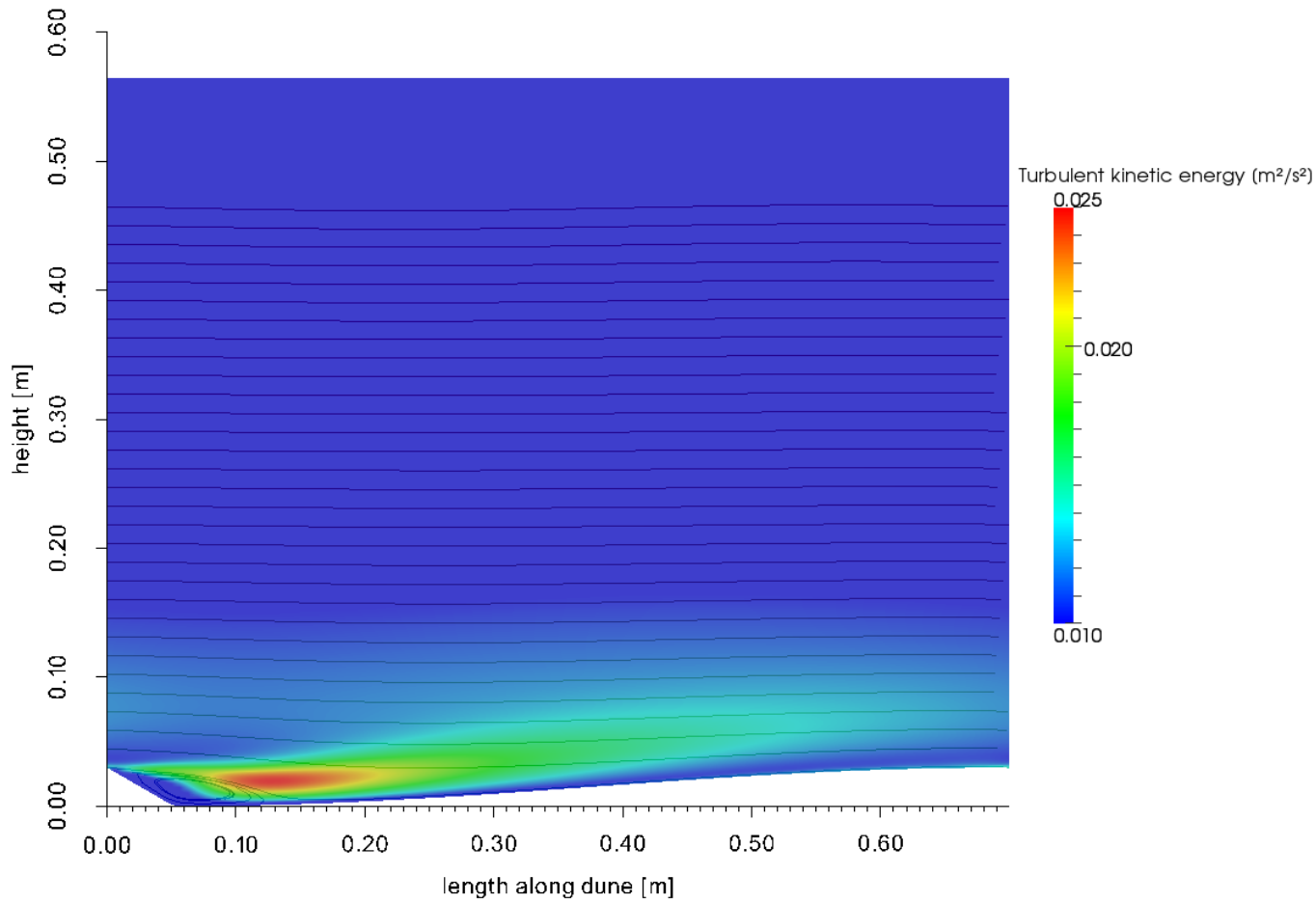
Figure 4.8: Case 1 - Secondary dune: Turbulent kinetic energy

4.3.3 Case 2 - Primary dune

Flow over the primary dune shows the same aspects of the flow like the secondary dune case (case 1). In the trough of the dune flow separation occurs (figure 4.9) and the TKE plot (figure 4.10) shows that a high intensity of turbulence located behind the flow separation zone. However, the dimensions of the primary dune are much larger than the secondary dune case. The primary dune is about three times higher and six times longer. The TKE plot shows that the high turbulent region is about eight times longer for the primary dune case in perspective to the secondary dune case.
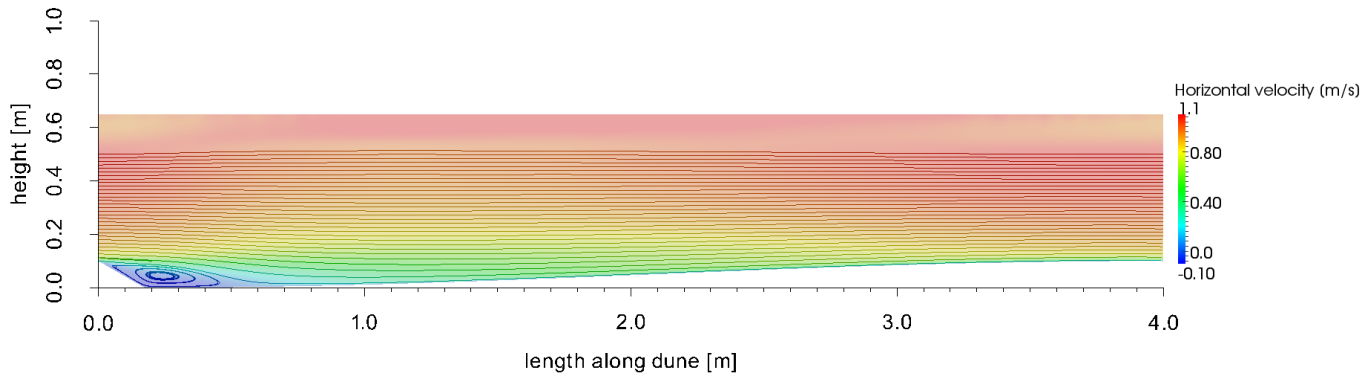
Figure 4.9: Case 2 - Primary dune: Horizontal velocities and streamlines
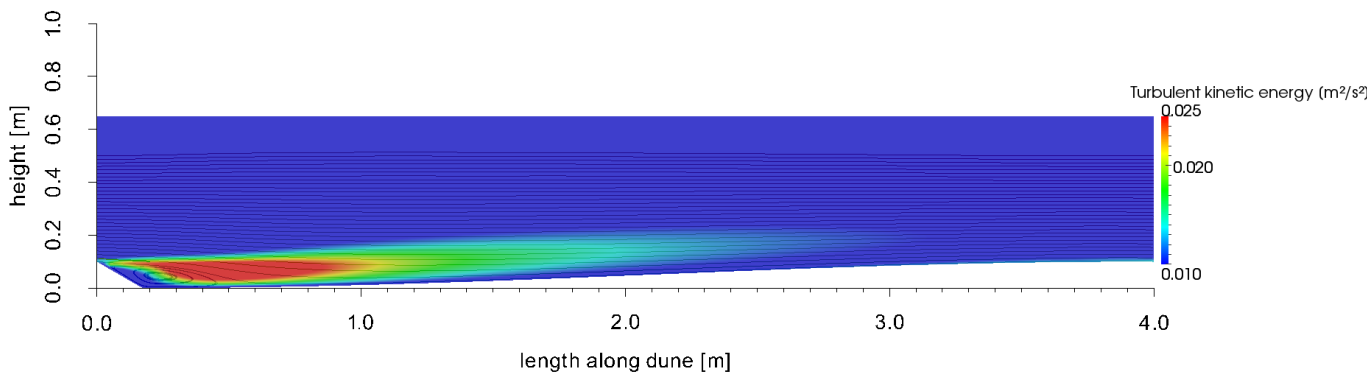
Figure 4.10: Case 2 - Primary dune: Turbulent kinetic energy

4.3.4   Case 3 - Primary dune and secondary dunes

The simulation of flow over the combination of primary and secondary dunes shows that in all troughs of the dune shapes flow separation occurs (figure 4.11). However, the intensity of the turbulent regions varies for the different secondary dunes (figure 4.12). Secondary dunes placed low on the stoss side of the primary dune induce a lower TKE than secondary dunes located more towards the crest of the primary dune. The secondary dune closest to the primary dune crest shows to induce similar or slightly higher turbulent intensities compared to the secondary dune case (case 1).

The turbulent region induced by the flow separation zone of the primary dune part has a lower intensity than to the primary dune case (case 2). However, the size of the wake of the turbulent region is similar.
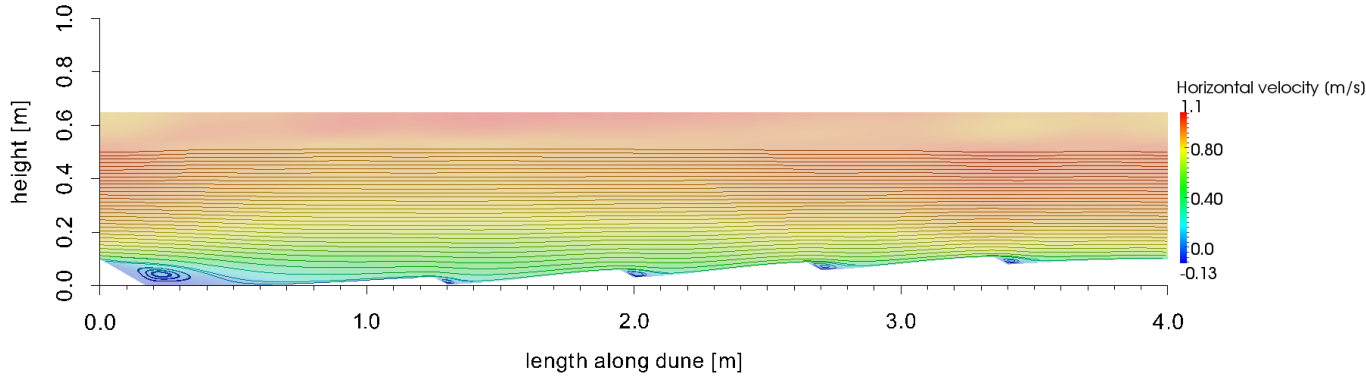
Figure 4.11: Case 3 - Primary dune containing secondary dunes: Horizontal velocities and streamlines
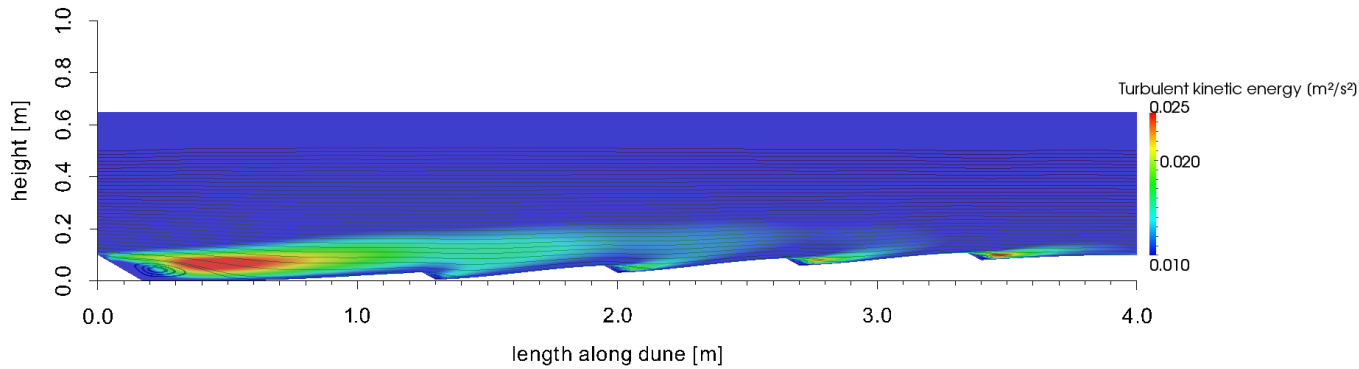
Figure 4.12: Case 3 - Primary dune containing secondary dunes: Turbulent kinetic energy

4.4 Form drag of the experimental dune configurations

The form drag of the experimental dune configuration is derived in this section. Form drag is defined by the difference in total roughness and grain roughness (section 2.3).

The flow velocity of the experimental cases is used to derive total roughness (equation 2.12). Grain roughness for the dune configurations is obtained from the flat bed case (case 0). The grain roughness for dune configurations is not corrected for bed form influences (e.g. the flow separation zone or increased surface length) since the form drag is generally dominant over the grain roughness (Knighton (1998) and Julien et al. (2002)). The dominance of form drag over grain roughness is also confirmed by results of the experimental dune configurations (figure 4.13) and by the grain roughness sensitivity analysis (appendix G). Therefore it is assumed the grain roughness is not influenced by the presence of bed forms and is directly obtained from the flat bed case (case 0). The derived total roughness of the experimental cases is shown in figure 4.13.

Form drag is derived by subtracting grain roughness from the total roughness. The form drag of the dune configurations is shown in figure 4.1. The combination of primary and secondary dunes (case 3) induces the largest amount of form drag, followed by the form drag induced by the primary dune (case 2). The secondary dune case (case 1) has the lowest form drag. Figure 4.1 also shows that the form drag of dune case 3 is larger than
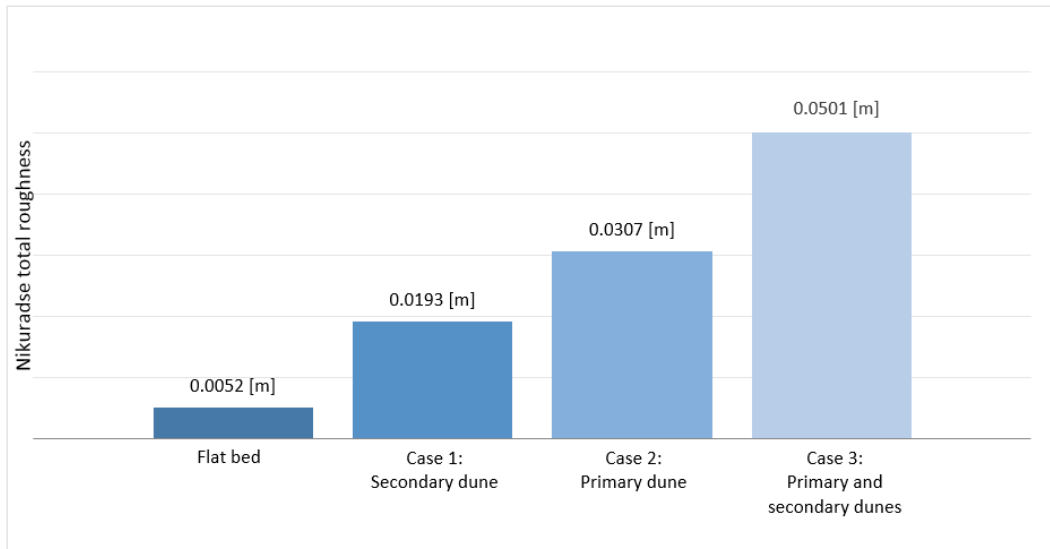
Figure 4.13: Total Nikuradse roughness of the three dune cases and the flat bed case

the summation of form drag induced by the separated dune shapes (case 1 and case 2).
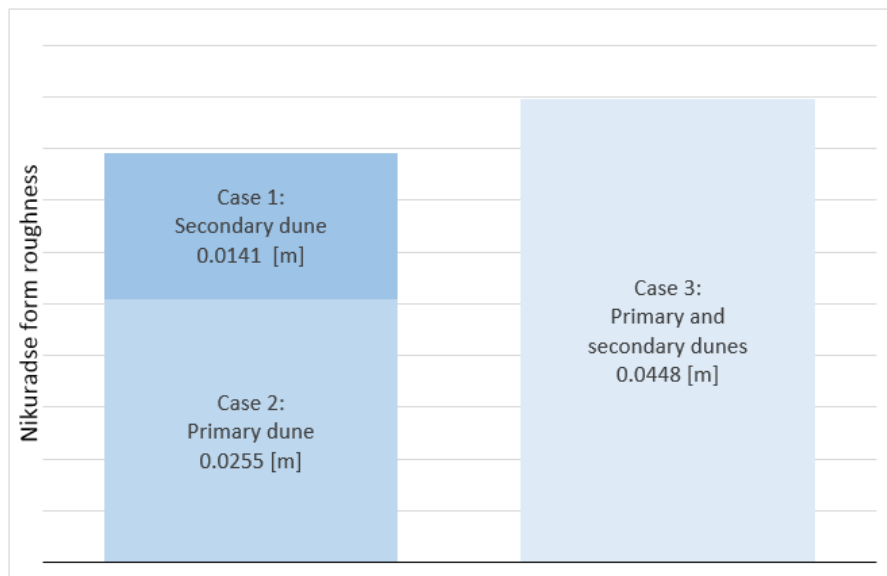
Table 4.1: Nikuradse form drag of the experimental dune configurations

Chapter 5

Discussion

In the introduction (chapter 1) the principles of grain roughness and form drag were discussed. The highly changing bed forms of the proposed bed form evolution process of Warmink et al. (2012) indicated that form drag during flood waves is likely to change. Three typical dune configuration were defined (chapter 4) which are related to the bed form stages defined in the proposed bed form evolution process. By flow modelling over these dune configuration the form drag is determined based on the occurring flow velocities.

This chapter couples the experimental results to the proposed bed form evolution process. Besides, the most important assumptions of the model and proposed improvements of the model set up are discussed.

5.1   Roughness variability during flood waves

The proposed bed form evolution process visualised in figure 1.2 consists of six separated bed form stages. The results of the three modelled dune configurations are used to describe the total roughness variation through these stages.

5.1.1   Form drag of bed form evolution stage 1, 2 and 3

The first two stages of the proposed dune evolution process show how smaller dunes increase in length and height, while the discharge increases. The third stage shows that this process continuous until the peak discharge has just passed.

Bed forms of the first and third stage are comparable to respectively the secondary dune (case 1) and primary dune (case 2) configuration (chapter 4). Comparing the flow separation zones of the secondary and primary dune (figure 4.7 and 4.9), the flow separation zone of the primary dune is about 4 times the size of the flow separation zone of the secondary dune. Besides, the flow separation zone of the secondary dune is steeper (about 4 to 5 times the secondary dune height) than the flow separation zone of the primary dune (about 6 times the primary dune height). Lefebvre et al. (2013) also observed that smaller bed forms generate shorter and steeper flow separation zones.

Based on the flow separation zones the form drag is expected to be larger for the primary dune (case 2) than the secondary dune (case 1) configuration. This is confirmed by figure

4.1 which shows that the primary dune configuration induces about 1.8 times the form drag of the secondary dune configuration. This factor is slightly smaller for the total roughness: about 1.6 (figure 4.13). Julien et al. (2002) measured an increase of total roughness with increasing discharge, which is also attributed to bed form height. Therefore it is concluded the form drag and total roughness increases for the first three stages of the bed form evolution process due to the increase of form drag.

5.1.2   Form drag of bed form evolution stage 4, 5 and 6

The last three stages of the proposed bed form evolution process represent the behaviour of bed forms during the falling stage of the flood. The large primary dunes from the third stage still increase in length but decrease in height during these last stages. In the fifth and the sixth stage the angle of repose of the primary dune lowers and secondary dunes migrate on top of the primary dunes.

The primary dune containing secondary dunes (case 3) configuration (chapter 4) is comparable to the fifth and sixth stage of the proposed bed form evolution process. The primary shape of dune case 3 is similar to dune case 2, while the secondary shapes were obtained from dune case 1. Therefore, the primary dune shape of this dune configuration does not show the lowering in angle and increase in length proposed by the bed form evolution process. However, the dune configuration of case 3 does reveal the influence of secondary dunes submerged on primary dunes.

Figure 4.11 shows that flow separation is present for all troughs of the primary and secondary dune shapes. However, the streamlines are not accurate enough to distinguish differences in flow separation zones in comparison to case 1 and case 2. From the TKE depicted in figure 4.12 differences are more clearly seen to the secondary dune case 1 (figure 4.8) and primary dune case 2 (figure 4.10). The intensity of TKE appears to be higher in the troughs of separately modelled dunes in case 1 and case 2 compared to the intensity of TKE of the troughs in case 3. However, the submerged secondary dune closest to the top of the primary shape shows about the same TKE as the secondary dune shape of case 1. This can be explained by the higher velocities over this secondary dune compared to the lower placed secondary dunes (figure 4.11). Fernandez et al. (2006) show that if secondary bed forms are even closer to the top of the primary bed form, interaction of the flow separation zones may occur which lead to high levels of turbulence intensity. Therefore the location of secondary dunes on the primary shape shows to be important for the intensity of the TKE.

Figure 4.1 shows that case 3 induced the highest form drag of all experimental dune configurations. The form drag of case 3 is even higher (approximately 1.1 times) than summation of the form drag of case 1 and case 2. In comparison to the primary dune (case 2) form drag is multiplied by a factor of about 1.8 if the same dune consists of merged secondary dunes. For total roughness this factor is about 1.6 (based on figure 4.13).

Total roughness of the bed forms occurring in the fifth and sixth stage of the proposed bed form evolution process may therefore still increase. However, following the bed form evolution process the primary shape in these stages lowers and flattens. This effect in not included in case 3 but may decrease the total roughness substantially (Best, 2002). Therefore simulations or measurements of additional dune configurations are required to understand the variations of form drag in the fifth and sixth stage.

5.2 Model assumptions

In order to put the conclusions and statements of this chapter in the right perspective, important assumptions and decisions of the model and the dune configurations are summarized in this section. Discussed is how these assumptions and decisions may influence the form roughness of the 6 stages of the bed form evolution process.

5.2.1 Laboratory scale versus field scale

The dune configurations, grain roughness, slope and water depth were all scaled to laboratory dimensions. The model results of the experimental dune configurations are reliable, since similar model settings and dimensions were used for the model validation. On the other hand, the question arises if the flow predicted by a laboratory scale model is representative for field scale conditions. In general for laboratory conditions the grain roughness and water depth are relatively small while the slope is relatively steep. For the field scale conditions it is generally the other way around.

The work of Lefebvre et al. (2013) shows a scaling method for the laboratory and field scale dimensions. The scaling reveals for which field scale dimensions the results of the laboratory scale apply. The scaling method consists of scaling all model properties (i.e. water depth, grain roughness, dune height, dune length) by a certain factor except for the slope. The slope is scaled in the counter direction. Using this method, the shear velocities at laboratory and field scale dimensions are similar.

In table 5.1 case 3 (chapter 4) is used as an example to show which field scale dimensions apply to the results of the laboratory scale model. Therefore a scaling factor of 10 is used. This is the same factor as used in chapter 4 to scale the field dune dimensions to laboratory scale dimensions. Table 5.1 shows that the dune dimensions and river slope are of the magnitude measured by Julien et al. (2002) and Wilbers and Ten Brinke (2003). However, the scaled grain roughness is relatively high and the water depth relatively small compared to measured river conditions.

The validity of the scaled grain and total roughness parameters is checked using one of the simplest roughness estimators, the roughness model of van Rijn (1993). The mathematical definition of the roughness parameter is given by equation 5.1. Using the field scale dimensions of the dune configurations (scaling factor of 10 is used) the roughness estimator overestimates the total roughness for all cases (table 5.2). The increase in total roughness when moving from case 1 to case 3 is however confirmed. The roughness model of van Rijn (1993) may be based on different dune shapes and flow conditions which could explain the differences. However, based on the comparison in table 5.2 the validity of the model results for field scale conditions can not be confirmed. Although the order of magnitude of the modelled total roughness shows to be reasonable.

$$k_N = k'_N + k''_{N,p} + k''_{N,s} \qquad\qquad (5.1)$$

$k_N = total\ Nikuradse\ roughness\ [m]$
$k'_N = D_{90}\ [m]\ (assumption:\ D_{90} = k_s grain)$
$k''_{N,p} = 1.1\delta_p(1 - e^(- 25\delta_p/\lambda_p))\ (Nikuradse\ roughness\ due\ primary\ dunes)$
$k''_{N,s} = 1.1\delta_s(1 - e^(- 25\delta_s/\lambda_s))\ (Nikuradse\ roughness\ due\ secondary\ dunes)$
$\delta = dune\ height\ [m]$
$\lambda = dune\ length\ [m]$

Table 5.1: Scaling of dune configuration case 3 to field scale conditions

		Case 3 - Laboratory scale conditions	Case 3 - Field scale conditions
Primary dunes	length	4.00 [m]	40.00 [m]
	height	0.10 [m]	1.00 [m]
Secondary dunes	length	0.70 [m]	7.00 [m]
	height	0.03 [m]	0.30 [m]
Water depth		0.45 [m]	4.50 [m]
Slope		0.0010 [-]	0.0001 [-]
k_s grain		0.0052 [m]	0.0520 [m]
k_s form		0.045 [m]	0.450 [m]

Table 5.2: Comparison of scaled roughness of the dune configurations and the roughness estimation based on equation 5.1

Dune configurations in field scale			Roughness estimation		Modelled roughness (scaled)	
grain roughness [m]		0.05	k'_N	0.054 m	0.052 m
primary dune	height (Δ) [m]	1.0	$k''_{N,p}$	0.511 m	0.255 m
	length (Λ) [m]	40.0			
secondary dune	height (Δ) [m]	0.3	$k''_{N,s}$	0.217 m	0.141 m
	length (Λ) [m]	7.0			
Total roughness case 1			k_N	0.271 m	0.193 m
Total roughness case 2			k_N	0.565 m	0.307 m
Total roughness case 3			k_N	0.782 m	0.501 m

5.2.2 Static and idealized shaped bed forms

The shapes of all dune configuration are idealized bed forms, consisting of a sinusoidal stoss side and a 30∘ lee side angle. Besides the bed forms are static (no migration) and sediment transport is not part of the model. The static bed forms are in contradiction to the bed being in constant movement (chapter 1). However, due the relatively slow morphological process it is appropriate to neglect this effect.

The assumption of the typical asymmetrical dune shape consisting of an angle of repose of 30∘ is believed to have a high impact on the form drag. Best (2002) discuss that in many models of alluvial dunes these typical bed form shapes are assumed, while most dunes in large sand bed rivers possess more symmetrical profiles, lower lee side angles, and flow separation that is either intermittent or absent. Many river bed forms would show no permanent flow separation and the turbulent region behind the bed forms would be much lower. Therefore it is arguable if the shapes of the experimental dune configurations (chapter 4) are representative for real bed forms in rivers. Nevertheless, these dune configurations show till which extent the roughness of form drag may reach.

5.2.3 2DV model versus 3D reality

In this research the width directional dimension of the flow is neglected and only the effect of two dimensional dune configurations is studied. However, in rivers the dunes vary in height and length, as well as in the width directional dimension. Therefore the 2DV flow pattern along this dimension change as result of the change in bed form shape. Besides, 2DH (horizontal plane) flow patterns become important as well.

The experiments of Maddux et al. (2003) show that averaged friction coefficients for flow over 3D (primary) bed forms was 50% higher than for the 2D shapes. However, despite the larger friction of the 3D dunes, the turbulence generated by them was much weaker. The increase in friction coefficients is contributed to the higher spatial variability in near-bed velocities and to the non-linear increase in skin friction induced by local high velocities. Grigoriadis et al. (2009) also shows different turbulent structures arising for 3D (primary) dune shapes. They used a large-eddy simulation to reveal spanwise roller coherent structures to develop because of separation at the dune crest. However, at the reattachment point they found horseshoe structures. Venditti (2007) shows both an increase and decrease of the flow separation zone of 3D (primary) bed forms compared to flow over 2D dune shapes. The magnitude of the flow separation of saddle shaped bed forms was lower than the flow separation over a lobe.

This research consists of a first exploration to secondary bed forms in 2DV. However, while the understanding of primary and secondary bed forms increases, the 3D modelling of primary and secondary dunes may be part of future research.

5.3   Improvements of the model set up

Several improvements to the free surface OpenFOAM model are proposed in this section.

Regarding the reliability of the model it is important a comprehensive study to the mesh sensitivity and the optimum mesh settings for free surface modelling in OpenFOAM is performed. To further improve confidence in the model a validation based on measurements of a dune profile consisting of merged secondary dunes is useful. The performed validation in chapter 3 exists of only single dune profiles and it remains unknown if the more complex case 3 of the dune configuration is accurately modelled.

Another improvement refers to the way in which the model is used for determining the form drag. For computing the flow properties of the different dune configurations, each time the slope (horizontal bodyforce) is predefined in the model. Therefore the shear velocity and bed shear stress do not change for the different cases. Only the velocities or discharge (since the water depth is remained) change as effect of the differences in form drag. However, for real river cases it is the discharge which always is assumed to be remained. Therefore a general hydrodynamic model setup consists of a discharge inlet and a controlled water level outlet. In order to maintain the benefits of the cyclic model but include a constant discharge, the slope (horizontal bodyforce) should be adjusted for each case until a certain discharge is achieved. In this way the cyclic model can be used to show the differences in total shear stress for each dune configuration.

Chapter 6

Conclusions and outlook

The first chapter defined the research objective: 'To provide a better understanding of the roughness variability during flood waves, by computing the form drag of typical primary and secondary dune configurations in rivers'. The research questions were used to fulfil this objective. Section 6.1 shortly recaps each research question and summarizes the important conclusions. An outlook for additional research is given in section 6.2.

6.1 Conclusions

Which model settings are used for creating a free surface model in OpenFOAM?
In chapter 2 the model settings are explained. The interFoam solver is selected to create a free surface flow while the k-epsilon turbulence model is used for simulating the turbulence aspects of the model. In order to able to work with a small model domain, cyclic boundary conditions are implemented for which the interFoam solver is adapted to work properly. Two mesh restrictions show to be important for flow modelling in OpenFOAM. The y^+ values should have a minimum value of 30 in order to properly model the grain roughness. For the same reason the ratio of the height of the cell centre to the grain roughness k_s should not exceed the value of 0.2.

How do the model results compare to a validation reference case?
The validation of the model is subject of chapter 3. The flat bed validation shows to fit the logarithmic velocity profile well and the grain roughness parameters obtained from the flow properties were in accordance to the input grain roughness of the model. The dune validation is carried out by comparing the model results to a laboratory experiment. However, grain roughness was not defined for these experiments. Therefore one laboratory experiment is used for calibration of the grain roughness. The actual validation of a second dune case was successful and shows a high agreement in measured and modelled velocity profiles, flow separation zones and total roughness parameters. Therefore it is concluded the model performs properly for modelling free surface flow.

What is the form drag of the investigated dune configurations?
The simulation of the flow over the experimental dune configurations is part of chapter 4. Long and high primary dunes (case 2) induce a higher form drag than the smaller and lower secondary dunes (case 1). However, the dune configuration consisting of both primary and secondary dunes (case 3) shows to induce the highest form drag. The form

drag of case 3 is even higher than the summation of the form drag of case 1 and cases 2. However, this does not directly follow from the turbulent kinetic energy plots. The TKE induced behind the trough of the primary dune shape of case 3 is lower than the similar primary dune shape of case 2. The secondary dune shapes of case 3 show divergent TKE intensities behind their troughs. The TKE intensities increase from the 1st secondary dune (close to the trough of the primary bed form) towards the last secondary dune close to the crest of the primary bed form. The first three secondary bed forms induce a lower TKE compared to case 1, while the last secondary dune induces approximately the same amount of turbulence in perspective to case 1.

What are the variations in form drag during floods, following the proposed model of bedform evolution?
Chapter 5 discusses the results of the experimental dune configurations in perspective to the variances of the form drag during the floods using the proposed bed form evolution process. Figure 1.2 refers to the bed evolution process consisting of six bed form stages. For the first three stages where the primary dunes are growing in both length and height is concluded that the form drag increases. For the last three stages, where the primary dune keeps increasing in length but decreases in height and secondary dunes start to occur, is concluded that it is possible for these dune configurations to induce a higher form drag than the high primary dunes of the 3th stage. The investigated dune configurations show form drag increases by a factor of 1.8 when secondary dunes occur on the primary dune. Therefore, secondary dunes merged on primary dunes add a significant amount of form drag, but the effect of decay of primary dunes in these stages is not determined. It depends on actual primary and secondary bed form shape and dimensions if form drag increases or decreases during the falling stage of a flood wave.

6.2   Outlook

The conclusions of this research are based on an exploratory investigation to form drag of primary and secondary dune configurations. Therefore many aspects of the dune shape and dimensions are not varied even though these definitely have their influence on the form drag. This section discusses the areas in which research should be continued to verify the applicability of the stated conclusions and gain a better understanding of the form drag during floods.

This research shows that the influence of primary and secondary bed forms are important for the development of turbulences inducing form drag to the flow. Nevertheless there is yet much to discover about primary bed forms and superimposed secondary bed forms. Changes in shape and dimensions of both the primary and superimposed secondary bed forms should be researched in order to improve the understanding of form drag during floods. Besides the influence of variations to the location of the superimposed secondary bed forms may be studied, which show to be important for the amount of turbulence induced by the superimposed secondary bed form. Actual knowledge of these influences is for now insufficient to fully understand form drag variations during the bed evolution process. In general, more dune configurations should be researched in order to these form drag variations.

In future research 3D modelling may also be considered. Measurements (i.e. Venditti (2007) and Maddux et al. (2003)) and 3D modelling (Grigoriadis et al., 2009) already show for some primary bed form cases the total roughness by the 2D shapes is underestimated.

However, 3D modelling is complex and time consuming due high computer processor requirements.

This research shows the form drag of primary and superimposed secondary bed forms is of high importance to total roughness of rivers. Proposed additional research may lead to better understanding and prediction of total roughness of specific dune configurations. This information could then be used to implement variable roughness parameters in the numerical models predicting the design water levels (chapter 1).

Bibliography

Best, J. (2002). An experimental study of turbulent flow over a low-angle dune. *Journal of Geophysical Research*, 107(C9):3135.

Best, J. (2005). The fluid dynamics of river dunes: A review and some future research directions. *Journal of Geophysical Research*, 110(F4):F04S02.

Booij, R. (1992). *TURBULENTIE in de waterloopkunde*. Technische Universiteit Delft.

Engelund, F. (1967). *A monograph on sediment transport in alluvial streams by Frank Engelund and Eggert Hansen*. Teknisk Forlag.

Fernandez, R., Best, J., and López, F. (2006). Mean flow, turbulence structure, and bed form superimposition across the ripple-dune transition. *Water Resources Research*, 42(5).

Grigoriadis, D. G. E., Balaras, E., and Dimas, a. a. (2009). Large-eddy simulations of unidirectional water flow over dunes. *Journal of Geophysical Research*, 114(F2):F02022.

Julien, P. Y., M.ASCE, Klaassen, G. J., Brinke, W. B. M. T., and Wilbers, A. W. E. (2002). Case Study : Bed Resistance of Rhine River during 1998 Flood. *Journal of Hydraulic Engineering*, 128(12):1042–1050.

Knighton, D. (1998). *Fluvial Forms and Processes: A New Perspective*. A Hodder Arnold Publication. Arnold.

Kundu, S. and Ghoshal, K. (2012). Velocity Distribution in Open Channels : Combination of Log-law and Parabolic-law. *World Academy of Science, Engineering and Technology*, 68:1735–1742.

Lefebvre, A., Paarlberg, A. J., and Winter, C. (2013). Flow separation and shear stress over angle of repose bedforms: a numerical investigation. *Water Resources Research*, 49(10).

Liu, X., García, M. H., and Asce, M. (2008). Three-Dimensional Numerical Model with Free Water Surface and Mesh Deformation for Local Sediment Scour. *Journal of Waterway, Port, Coastal, and Ocean Engineering*, (August):203–217.

Maddux, T. B., Nelson, J. M., and McLean, S. R. (2003). Turbulent flow over three-dimensional dunes: 1. Free surface and flow response. *Journal of Geophysical Research: Earth Surface*, 108(F1).

Martinez, B. (2011). *Wind resource in complex terrain with OpenFOAM*. PhD thesis, Technical University of Denmark.

McLean, S., Wolfe, S., and Nelson, J. (1999a). Predicting Boundary Shear Stress and Sediment Transport over Bed Forms. *Journal of Hydraulic Engineering*, 125(7):725–736.

McLean, S. R., Wolfe, S. R., and Nelson, J. M. (1999b). Spatially averaged flow over a wavy boundary revisited. *Journal of Geophysical Research: Oceans*, 104(C7):15743–15753.

Moradnia, P. (2010). CFD of Air Flow in Hydro Power Generators. Technical report, Chalmers University of Technology, Göteborg, Sweden.

Ogink, H. J. M. (1989). *Hydraulic Roughness of Single and Compound Bed Forms*. Delft Hydraulics.

OpenFOAM Foundation (2012). OpenFOAM, The Open Source CFD Toolbox - User Guide version 2.1.1. Technical report.

OpenFOAM Foundation (2013). Standard Solvers.

Paarlberg, A. J., Dohmen-Janssen, C. M., Hulscher, S. J. M. H., and Termes, P. (2007). A parameterization of flow separation over subaqueous dunes. *Water Resources Research*, 43(12):W12417.

Pattanapol, W., Wakes, S. J., Hilton, M. J., and Dickinson, K. J. M. (2007). Modeling of Surface Roughness for Flow Over a Complex Vegetated Surface. *Proceedings of world academy of science, engineering and technology*, 26(December).

Salim, S. M. and Cheah, S. C. (2009). Wall y + Strategy for Dealing with Wall-bounded Turbulent Flows. *Proceedings of the International MultiConference of Engineers and Computer Scientists*, II.

Van Rijn, L. C. (1984). Sediment transport, part {III:} bed forms and alluvial roughness. *Journal of Hydraulic Engineering*, 110(12):1733–1754.

van Rijn, L. C. (1993). *Principles of sediment transport in rivers, estuaries and coastal seas*. Number dl. 1 in Principles of Sediment Transport in Rivers, Estuaries, and Coastal Seas. Aqua Publications.

Venditti, J. G. (2007). Turbulent flow and drag over fixed two- and three-dimensional dunes. *Journal of Geophysical Research*, 112(F4):F04008.

Warmink, J., Dohmen-Janssen, C., and Schielen, R. (2012). Bed form evolution under varying discharges, flume versus field. In *River Flow 2012*, pages 183–190. CRC Press.

Wilbers, A. and Ten Brinke, W. (2003). The response of subaqueous dunes to floods in sand and gravel bed reaches of the Dutch Rhine. *Sedimentology*, 50(6):1013–1034.

Appendix A

Technical details boundary conditions

The technical details of the boundary conditions used in the OpenFOAM model are summarized in table A.1. Most of the settings (including the numerical scheme) are obtained from the 'dam break' tutorial of OpenFOAM Foundation (2012).

Table A.1: Technical details of the used boundary conditions in the OpenFOAM model

		bottom					
		U	k	epsilon	nut	p_rgh	alpha1
flatbed	case 1a,2,3,4a,4b	fixedValue uniform (0,0,0)	kqRWall-Function	epsilon-WallFunction	nutkRoughWallFunction; Ks 0.01; Cs 0.327	buoyant-Pressure	zero-Gradient
flatbed	case 1b	fixedValue uniform (0,0,0)	kqRWall-Function	epsilon-WallFunction	nutkRoughWallFunction; Ks 0.00654; Cs 0.5	buoyant-Pressure	zero-Gradient
flatbed	case 1c	fixedValue uniform (0,0,0)	kqRWall-Function	epsilon-WallFunction	nutkRoughWallFunction; Ks 0.00327; Cs 1.0	buoyant-Pressure	zero-Gradient
dune	ML2/ML6 and experiments	fixedValue uniform (0,0,0)	kqRWall-Function	epsilon-WallFunction	nutkRoughWallFunction; Ks 0.00176274; Cs 1.0	buoyant-Pressure	zero-Gradient

		atmosphere					
		U	k	epsilon	nut	p_rgh	alpha1
flatbed	case 1a,2,3,4a,4b	zero-Gradient	inletOutlet; inletValue 1e-5	inletOutlet; inletValue 0.1	calculated	total-Pressure	inletOutlet; uniform 0
flatbed	case 1b	zero-Gradient	inletOutlet; inletValue 1e-5	inletOutlet; inletValue 0.1	calculated	total-Pressure	inletOutlet; uniform 0
flatbed	case 1c	zero-Gradient	inletOutlet; inletValue 1e-5	inletOutlet; inletValue 0.1	calculated	total-Pressure	inletOutlet; uniform 0
dune	ML2/ML6 and experiments	zero-Gradient	inletOutlet; inletValue 1e-5	inletOutlet; inletValue 0.1	calculated	total-Pressure	inletOutlet; uniform 0

Appendix B

Adapted interFoam solver

The full code of the adapted UEqn.h file of the interFoam solver is covered in figure B.1.

```cpp
    dimensionedVector bodyForce = dimensionedVector(mesh.thisDb
().lookupObject<dictionary>("transportProperties").lookup("bodyForce"));

    surfaceScalarField muEff
    (
        "muEff",
        twoPhaseProperties.muf()
      + fvc::interpolate(rho*turbulence->nut())
    );

    fvVectorMatrix UEqn
    (
        fvm::ddt(rho, U)
      + fvm::div(rhoPhi, U)
      - fvm::laplacian(muEff, U)
      - (fvc::grad(U) & fvc::grad(muEff))
    //- fvc::div(muEff*(fvc::interpolate(dev(fvc::grad(U))) & mesh.Sf()))
      - bodyForce*rho //Added 14-08-2013: Bodyforce for cyclic channel flow
    );

    UEqn.relax();

    if (pimple.momentumPredictor())
    {
        solve
        (
            UEqn
         ==
            fvc::reconstruct
            (
                (
                    fvc::interpolate(interface.sigmaK())*fvc::snGrad(alpha1)
                  - ghf*fvc::snGrad(rho)
                  - fvc::snGrad(p_rgh)
                ) * mesh.magSf()
            )
        );
    }
```

Figure B.1: Adapted UEqn.h file of the interFoam solver

Appendix C

Convergence of the solutions generated by the free surface OpenFOAM model

To ensure the output of the free surface model is converged the Courant numbers and the residuals of the solutions are monitored. The Courant numbers and residuals showed in figure C.1 and C are obtained from the same timestep as the output shown in chapter 3 and 4.

$z_0 = 0.00018$ [m]	Flatbed 1a	Flatbed 1b	Flatbed 1c	Flatbed 2	Flatbed 3	Flatbed 4a	Flatbed 4b
Courant nr. (max)	0.45	0.41	0.41	0.45	0.34	0.50	0.49
u_x	1.97E-09	1.38E-09	1.38E-09	3.56E-09	2.85E-09	8.66E-09	1.77E-09
u_z	1.34E-09	3.83E-09	3.83E-09	6.26E-09	2.57E-09	2.90E-09	4.40E-09
epsilon	1.53E-09	2.11E-09	2.11E-09	6.13E-09	1.92E-09	1.67E-09	6.48E-10
k	4.30E-10	1.09E-09	1.09E-09	6.20E-09	7.55E-10	9.03E-10	7.79E-09

Figure C.1: Residuals and Courant numbers of the flat bed validation

	validation		experiments			
$z_0 = 0.00018$ [m]	dune ML2	dune ML6	flatbed	case 1	case 2	case 3
Courant nr. (max)	0.50	0.45	0.42	0.50	0.50	0.50
u_x	1.26E-10	3.60E-09	7.43E-09	4.75E-09	2.35E-09	4.33E-09
u_z	4.34E-09	9.42E-09	2.56E-09	2.45E-10	3.12E-09	8.73E-09
epsilon	6.71E-09	1.91E-09	4.06E-10	3.16E-10	5.43E-09	2.17E-09
k	9.15E-10	2.72E-09	3.50E-09	4.64E-09	6.80E-09	6.65E-09

Table C.1: Residuals and Courant numbers of the dune validation and model experiments

Appendix D

Sensitivity analysis flat bed case

Several mesh adjustments to the flat bed case have been made in order to determine the mesh dependence of the model output. The meshes corresponding to the cases mentioned in chapter 3 are visualised in this appendix. The water depth in each of these models is set to 0.5 meter.
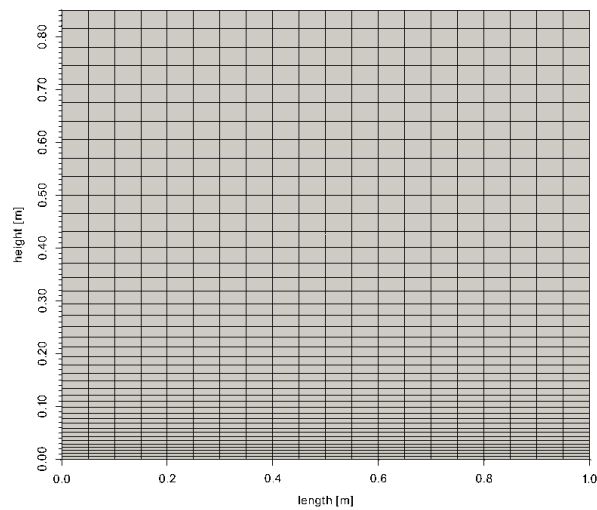
Figure D.1: Mesh used for flatbed 1a, 1b and 1c (varying roughness constant c_s)
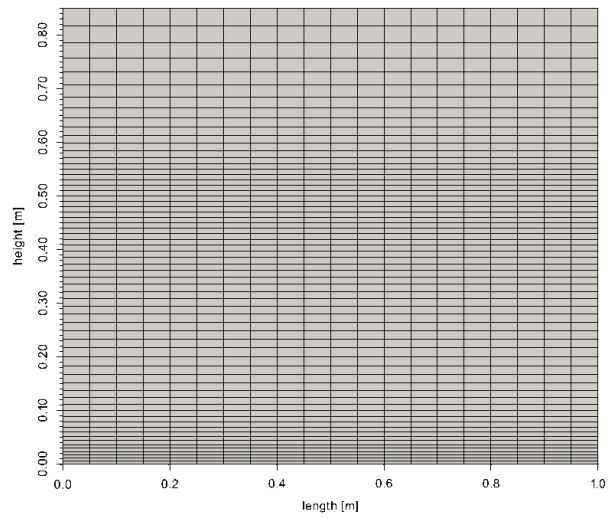
Figure D.2: Mesh used for flatbed 2 (surface refinement)
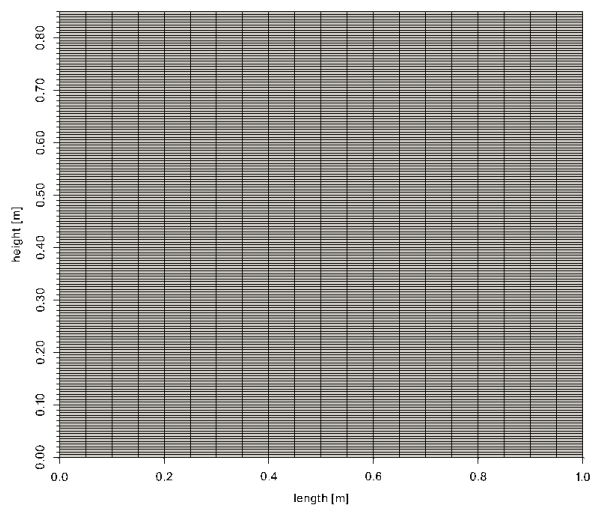
Figure D.3: Mesh used for flatbed 3 (total refinement)
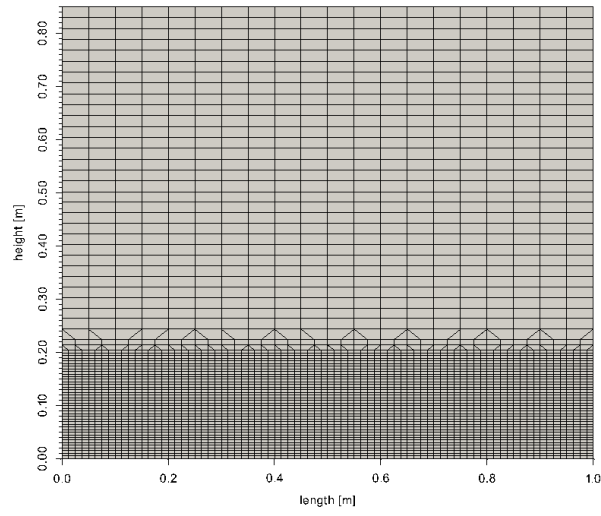
Figure D.4: Mesh used for flatbed 4a (bottom refinement using SnappyHexMesh)
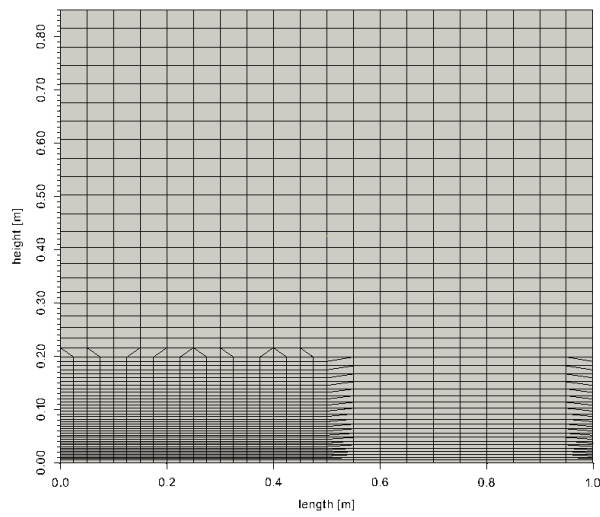
Figure D.5: Mesh used for flatbed 4b (partly bottom refinement using SnappyHexMesh)

Appendix E

Dune validation cases including Delft3D results

The Delft3D results achieved by Lefebvre et al. (2013) are added to the dune validation cases ML2 and ML6. Velocity profiles of both cases are compared in figure E.1 and E.3. The comparison of flow separation zones is shown in figure E.2 and E.4. The modelled Delft3D velocities near the bottom sometimes appear below the bed. This is likely the result of the Cartesian grid used by Lefebvre et al. (2013). Therefore diagonal bed shapes are modelled as a staircase.
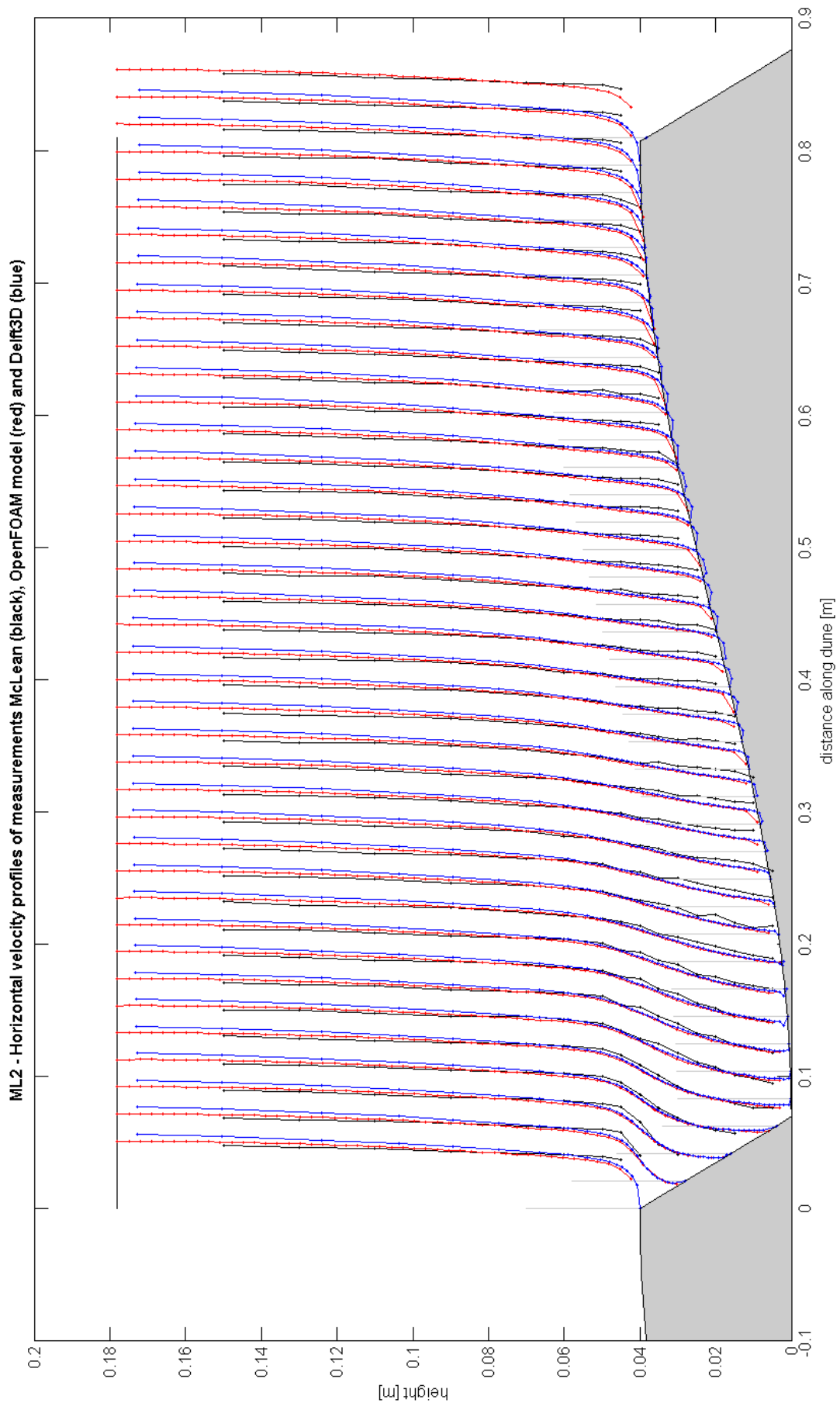
Figure E.1: ML2 - Velocity profiles of measurements of McLean (black), modelled by Delft3D (blue) and modelled by OpenFOAM (red). Velocities are scaled by a factor $\frac{1}{10}$.
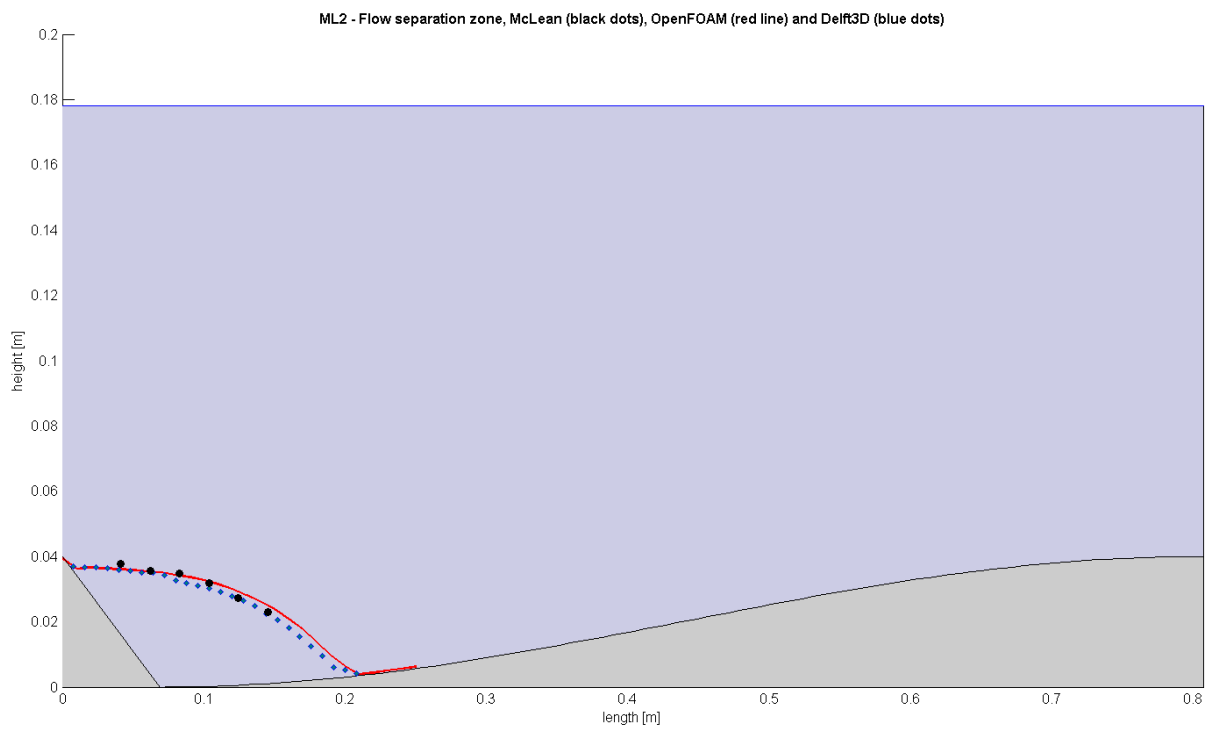
Figure E.2: ML2 - Flow separation zones of measurements of McLean (black dots), Delft3D (blue dots) and OpenFOAM (red line)
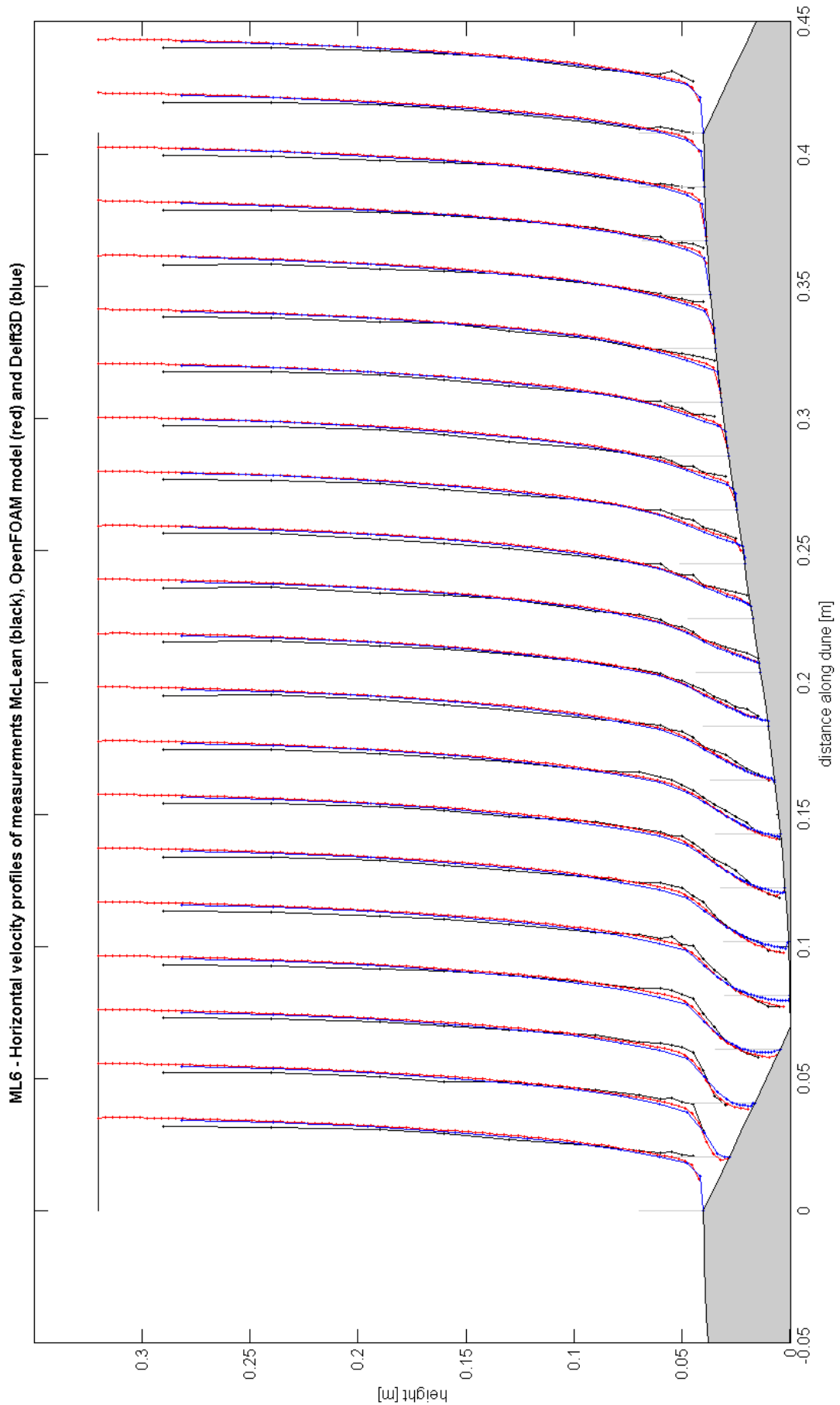
Figure E.3: ML6 - Velocity profiles of measurements of McLean (black), modelled by Delft3D (blue) and modelled by OpenFOAM (red). Velocities are scaled by a factor $\frac{1}{10}$.
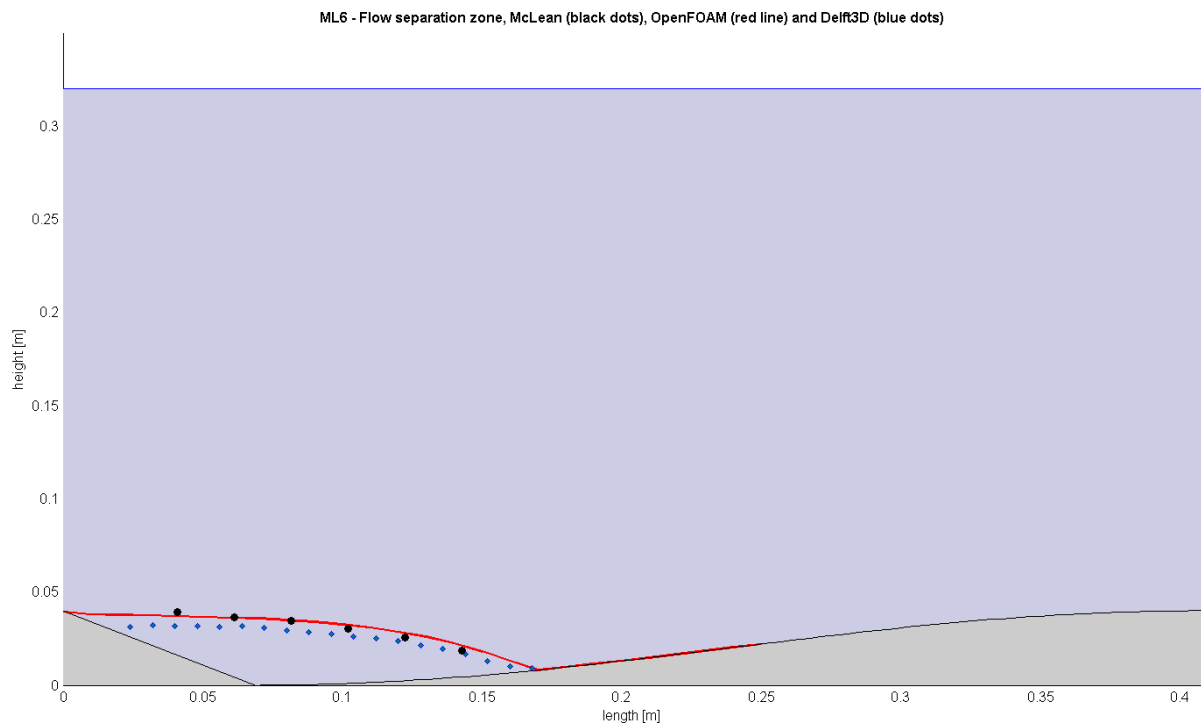
Figure E.4: ML6 - Flow separation zones of measurements of McLean (black dots), Delft3D (blue dots) and OpenFOAM (red line)

Appendix F

Constructed meshes for model experiments

The constructed meshes for all model experiments are depicted in figure F.2, F.3 and F.4.
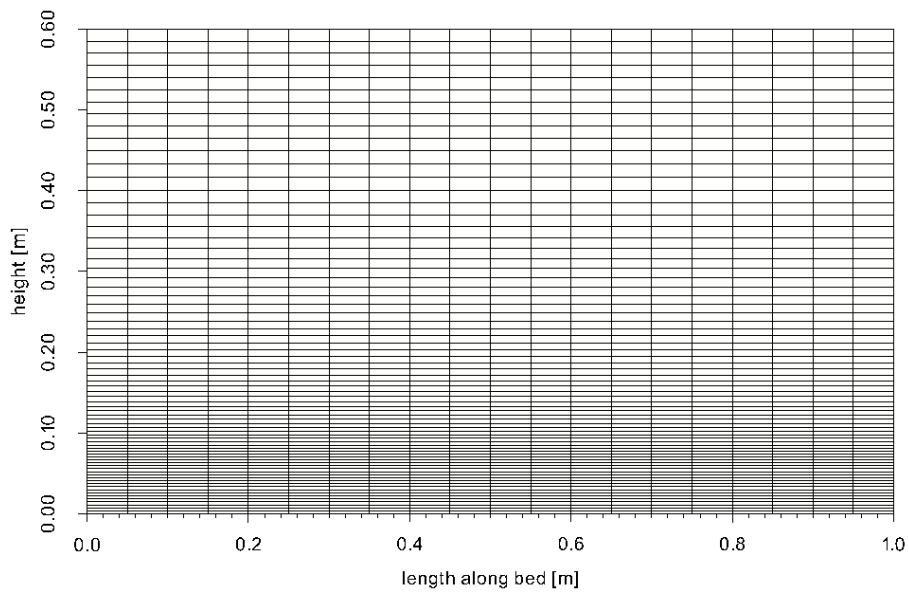
Figure F.1: Flatbed: Mesh
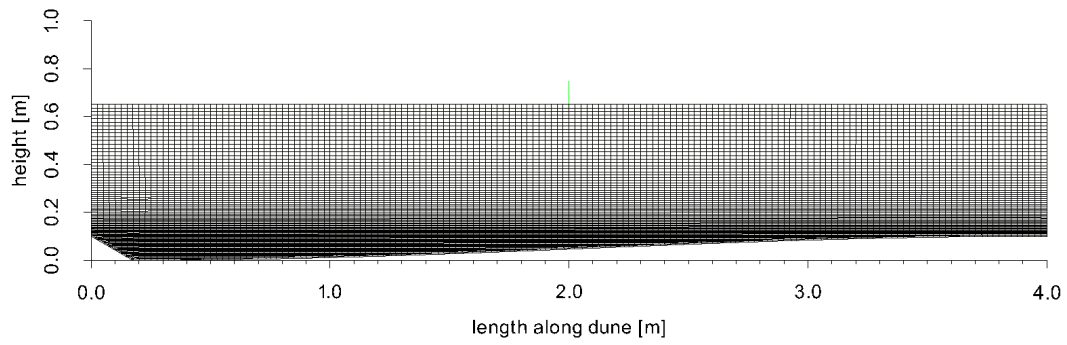
Figure F.2: Case 1 - Secondary dune: Mesh
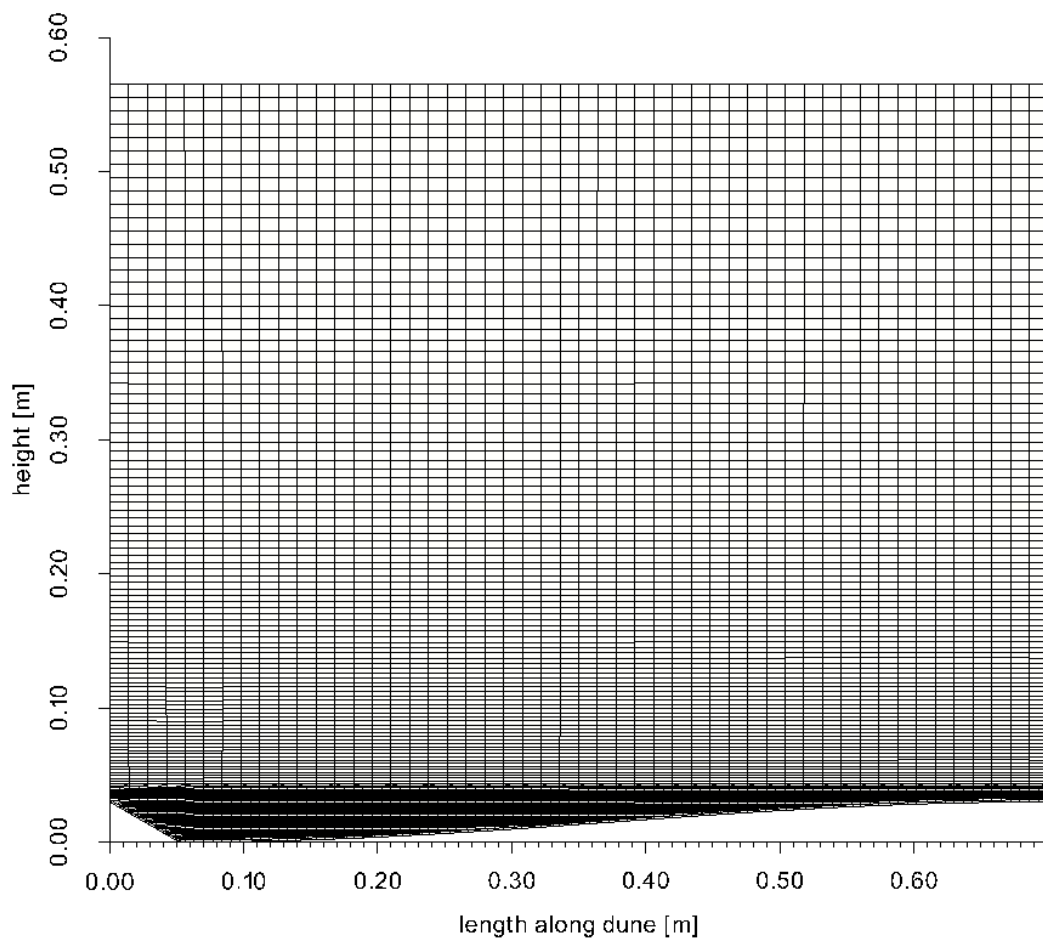
Figure F.3: Case 2 - Primary dune: Mesh
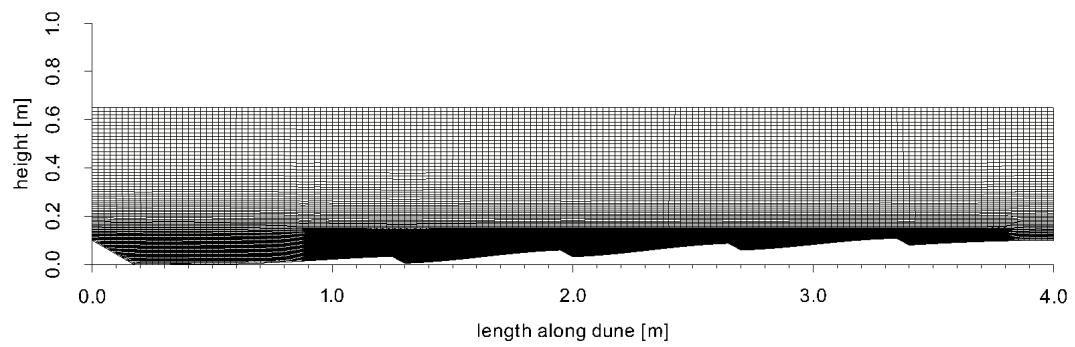
Figure F.4: Case 3 - Primary dune: Mesh

Appendix G

Sensitivity varying grain roughness

In order to gain insight in the sensitivity of the form drag to the grain roughness, the three dune cases are run again with a 20% higher and 20% lower grain roughness. Small changes in grain roughness are applied to be able to use the same mesh (see chapter 2.1.6 for mesh restrictions). Therefore no visual differences are noticed in figures of the horizontal flow velocities or turbulent kinetic energy, however they do slightly change.

- Grain roughness variations:
  $Decrease\ 20\%:\ z_0 = 0.000144\ [m]$
  $Default\ z_0 = 0.00018\ [m]$
  $Increase\ 20\%:\ z_0 = 0.000216\ [m]$

Table G.1 summarizes the sensitivity results of the flatbed case and dune configurations for variations in grain roughness. The flat bed case shows to model the change in grain roughness well. The total Nikuradse roughness (for the flat bed case the grain roughness) derived from velocities of the model shows a decrease and increase of 19% for respectively the smoother and rougher grain roughness.

Results of the dune configurations show an interesting pattern. For all dune cases, an increase in grain roughness also results in an increase in form roughness. Sensitivity of the form drag is however of a lower magnitude in perspective to the grain roughness variations. In general the form drag varies from around -8% to +12% in comparison to the $\pm 19\%$ variation of the grain roughness. Considering only case 3, containing the primary and secondary dunes, this sensitivity is reduced to about $\pm 5\%$.

Table G.1: Sensitivity of the average velocity, total roughness and form roughness in comparison to the variation of the grain roughness

		input		output		derived roughness from output			
		$k_{s\,grain}$ [m]	change	$\bar{U}$ [m/s]	change	$k_{s\,tot}$ [m]	change	$k_{s\,form}$ [m/s]	change
flat bed		0.00432	-20%	1.19	3.1%	0.0042	-19.1%		
		0.00540		1.15		0.0052			
		0.00648	20%	1.12	-2.5%	0.0062	19.2%		
dune	case 1	0.00432	-20%	0.95	2.0%	0.0172	-10.9%	0.0130	-7.8%
		0.00540		0.93		0.0193		0.0141	
		0.00648	20%	0.91	-2.4%	0.0220	14.2%	0.0158	12.4%
dune	case 2	0.00432	-20%	0.87	1.6%	0.0283	-8.0%	0.0240	-5.7%
		0.00540		0.86		0.0307		0.0255	
		0.00648	20%	0.84	-1.8%	0.0338	10.0%	0.0276	8.1%
dune	case 3	0.00432	-20%	0.79	1.4%	0.0468	-6.5%	0.0426	-5.0%
		0.00540		0.78		0.0501		0.0448	
		0.00648	20%	0.77	-1.4%	0.0534	6.7%	0.0472	5.2%